Nano Energy 41 (2017) 269–284

Contents lists available at ScienceDirect

Nano Energy

journal homepage: www.elsevier.com/locate/nanoen

Review

Solar water evaporation by black photothermal sheets

Guohua Liu[a,*], Jinliang Xu[b], Kaiying Wang[c]

[a] School of Energy and Power Engineering, Nanjing University of Science and Technology, Nanjing 210094, China
[b] State Key Laboratory of Alternate Electrical Power System with Renewable Energy Sources, North China Electric Power University, Beijing 102206, China
[c] Department of Micro and Nano Systems Technology, University College of Southeast Norway, Horten 3184, Norway

ARTICLE INFO

Keywords:
Solar energy
Water evaporation
Carbon materials
Plasmonic
Photothermal conversion

ABSTRACT

Solar energy-to-heat conversion for steam generation is an essential metrology for power generation, water purification and desalination. Harvesting light energy and converting it to heat as terminal energy by black photothermal sheets is a novel strategy to attain this goal. This technology rely on use of black nanomaterials as light absorber to increase the absorption and conversion efficiency of solar energy. Fundamental understanding of their structure-property has to be fully exploited for further developing efficient solar-to-heat systems. This report summarizes physical understanding and experimental advances in development of black photothermal sheets for solar water evaporation. We examine the popular photothermal systems with remarkable vapor generation performance to identify the state-of-the-art of the device design. Three groups of the photothermal sheet are discussed in terms of different light-harvesting materials, such as carbon-based sheets, plasmonic sheets as well as semiconducting sheets. The physical difference of these novel devices with their steam releasing property are also highlighted.

1. Introduction

Harvesting solar energy for steam generation is one of the most important strategies of green energy innovation because the technology underpin a broad range of applications, such as power generation, absorption chillers, desalination systems, water purification and sterilization systems [1–4]. Current technology of producing steam using solar energy rely on a surface to absorb solar irradiation, and transferring the accumulated heat to the bulk water directly or via an intermediate heat transfer fluid [5,6]. This requires high optical concentration and suffers from high optical loss and surface heat loss, or needs vacuum to reduce convective heat loss under moderate optical concentration, which add complexity and cost to the photothermal system. Therefore, there is a significant need to develop cost-effective and high efficient solar energy harvesting systems for vapor/steam generation.

Low-cost, micro/nanostructured photothermal systems with broadband light harvesting has recently been emerging as a promising approach. Fluids seeded with nanoparticles (NPs) as volumetric absorbers minimize the surface energy loss by uniform temperature in the fluid and enhance thermal conductivity, such as the dispersed Au NPs in water solution achieve a solar-thermal-conversion efficiency of 24% [7–9]. Nevertheless, a significant of the absorbing NPs in this situation is wasted due to absorption and scattering of the incident light by the NPs above [10]. To overcome the issue, floating sheets such as carbon-based foam, paper, porous anodic alumina and cellulose membrane have been suggested to localize the absorbing material on air-water interfaces for more efficient and cost-effective steam generation [11–16].

In these platforms, steam generation by heat localization is performed through a sequential cooperation of light absorbing, thermally insulating and capillary action (Fig. 1) [13,17–20]. Absorbers using various black materials, such as porous carbon materials, metallic plasmonic structures and semiconducting NPs are demonstrated for efficient solar absorption. The substrate for heat localization functioned as thermal insulator that reduce the heat transfer between vaporization region and bulk liquid. Due to the channel-capillary effect of the supports for water transport at negative pressures and steam escape (Fig. 2), localized evaporation is achieved with improved thermal efficiencies ~ 64% [20–24]. In addition, the use of solar concentrator further enhance the thermal efficiencies up to 85–90% [14,15,25]. However, how to build efficient solar-to-steam systems by use of absorbing nanomaterials and/or porous supports still remains a challenging goal.

In this work, we summarize physical understanding and experimental advances on development of black photothermal sheets for solar water evaporation. We firstly describe the physics of black material for light-to-heat conversion to illustrate conceptual development. The

* Corresponding author.
E-mail address: liuguohua126@126.com (G. Liu).

http://dx.doi.org/10.1016/j.nanoen.2017.09.005
Received 29 June 2017; Received in revised form 25 August 2017; Accepted 3 September 2017
Available online 22 September 2017

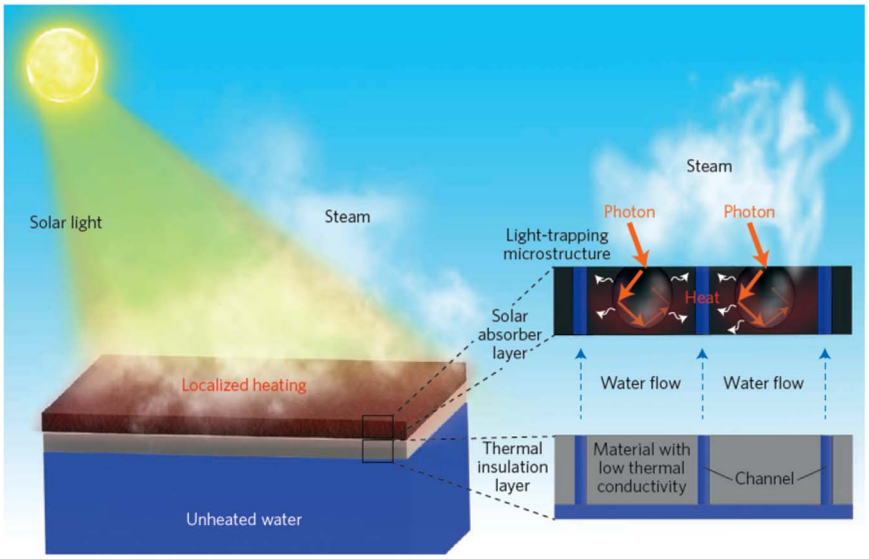

Fig. 1. The interfacial-photothermal sheet floating at air-water interface. Solar light harvesting by the absorber layer and then converted into thermal energy heats up the water at interface. The thermal insulation layer consists of material with low thermal conductivity and helps confine the heat at the interface. The channels within the thermal insulation layer and the absorber layer wick the beneath water to the hot interface for vapor generation. The insets show the conversion of photon energy to heat in the absorber layer and the transportation of water in both the absorber and the thermal insulation layer. Reproduced with permission [17]. Copyright 2017 Nature Publishing Group.

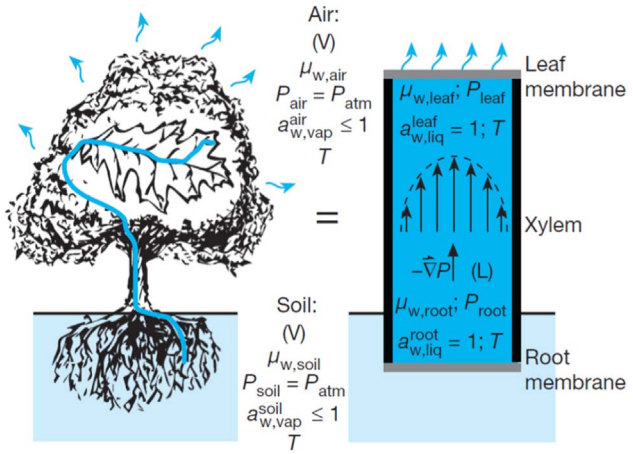

Fig. 2. Negative transpiration of liquid water. Water transport from the soil to the air in a tree and of a minimal model of the components. Water loss by evaporation reduces the liquid pressure within the leaf relative to atmospheric pressure, which wicks water out of the soil and up the xylem to preserve hydration. Reproduced with permission [22]. Copyright 2008 Nature Publishing Group.

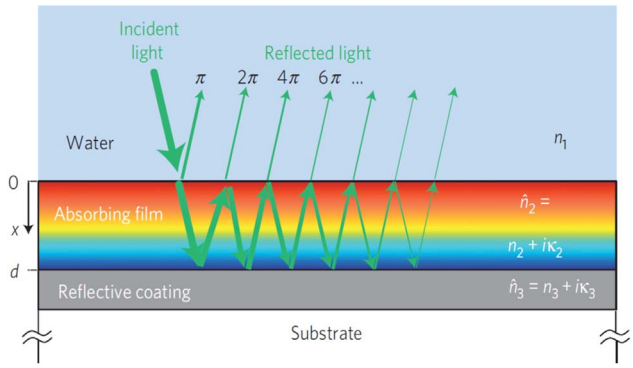

Fig. 3. Resonant light trapping in quarter-wave films. Reproduced with permission [27]. Copyright 2012 Nature Publishing Group.

solar-to-steam platforms are thus classified in terms of the light-harvesting materials, such as carbon-based sheets, plasmonic sheets as well as semiconducting sheets. We then discuss the photothermal sheets in particular form to identify state-of-the-art of the device design. The key factors yielding remarkable photothermal performance are also highlighted to distinguish the physical difference of devices. Finally, the report concludes with a summary on the current achievements and a few prospect on remaining challenges.

2. Physics of black material for light-to-heat conversion

Conversion of solar radiation into heat is normally achieved either by direct absorption in a heat transfer fluid, or indirectly by some kind of black absorbing surfaces from which the heat is collected and conducted to heat transfer fluid (Fig. 3) [26,27]. The heat generation process involves absorption of incident photons, and heat transfer from black materials to surrounding media. The heat releasing mechanism is that light-induced electric field drives mobile carriers inside crystals of the material, and the energy gained by carriers turns into heat. Then the heat diffuses away from materials leading to an increased temperature of surrounding medium [28]. Two parameters are normally used to assess the evaporation performance. The water evaporation rate is described by equation $\dot{m} = \frac{dm}{A \times dt}$, where m is the mass of evaporated water, t is time and A is the surface area of photothermal sheet. The solar thermal efficiency is calculated by the formula $\eta_{th} = \frac{Q_e}{Q_s} = \frac{\dot{m} h_{LV}}{C_{opt} q_i}$, where Q_s is the power of solar illumination and Q_e is the power for water evaporation, h_{LV} is the total enthalpy of liquid vapor phase change, C_{opt} is the optical concentration, and q_i is the normal direct solar irradiation. Particularly, the calculation of the total enthalpy of liquid-vapor phase change should consider both the sensible heat and the temperature-dependent enthalpy of vaporization.

There are many candidates for the absorber layers and mainly three types of photothermal agents are employed, e.g. carbon-based material, plasmonic metals and semiconducting materials. Amorphous carbon composed of a mixture of sp^2 and sp^3 bonding, is a carbonaceous solid that has no long-range crystalline order, and usually contains hydrogen and nitrogen. It has good ability in broad-band light absorption due to closely spaced energy levels of the loosely-held π electrons. Moreover, stability engendered by the aromatic bonds makes the material nearly inert at atmospheric temperatures and insoluble in water and many other solvents [29]. Conventional carbon black or graphite absorb visible light due to the π-band's optical transitions as well, while they are limited by a moderate reflection of 5–10% at air-dielectric interface [30]. An interesting approach to overcome the limit is to use nanostructures, especially vertically aligned carbon nanotubes or porous graphene [31–35]. By this way, large amount of optical microcavities are formed by reflecting faces on two sides of spacer layer, which confine light to small volumes by resonant recirculation that enhance interaction of light with the materials significantly [36].

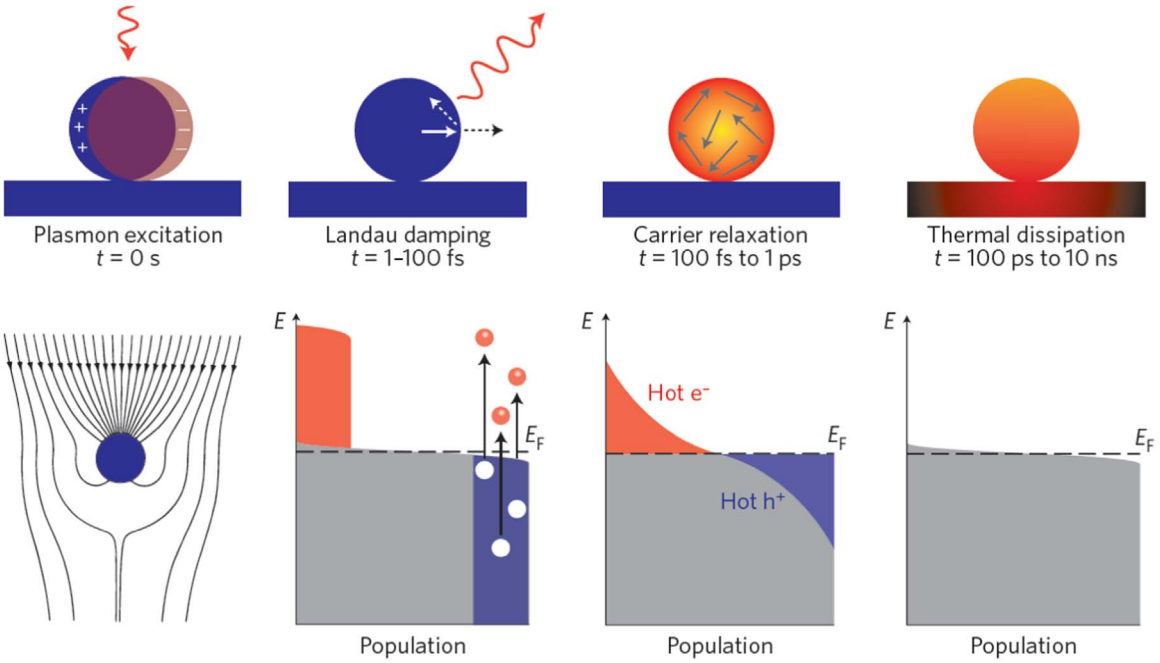

Fig. 4. Photoexcitation and subsequent relaxation processes following the illumination of a metal nanoparticle with a laser pulse, and characteristic timescales. Reproduced with permission [37]. Copyright 2015 Nature Publishing Group.

Heat generation becomes strong in case of metal NPs by plasmon resonance since they have many mobile electrons for the heat conversion. The plasmon resonance is a unique optical phenomenon occurring on metallic structures. When the frequency of incident light matches oscillation frequency of delocalized electrons in metals, it triggers a collective excitation of the electrons. These excited hot electrons oscillate coherently with incident electromagnetic field. This damping exerted on the free electron gas oscillating inside the particle results in heat generation by a Joule mechanism (Fig. 4) [37–39]. By electron-electron scattering processes, the hot carriers realize their energy redistribution within a fast timescale, which leads to remarkable heating of the plasmonic element itself. Following on a longer timescale, the local heat is further transferred from the plasmon-structure to its surrounding environment by thermal conduction [40].

Due to low cost and low cytotoxicity, black inorganic or organic semiconductors are new kinds of photothermal agents [16,41–44]. In these materials, heat generation is much weak since the heat dissipation fulfills through an interband absorption process with the excitation of a single electron and hole. The most photons from solar emission has higher energy than the bandgap of semiconductor, which leads to the creation of above-bandgap electron-hole pairs in the semiconductor under irradiation [16]. The above-bandgap electrons and holes then relax to the band edges and convert the extra energy into heat through a thermalization process (Fig. 5**a**). The relaxation dynamics of the above-bandgap charges could be quite complicated, but it may be dominated by an acoustic-phonon scattering mechanism [45]. This mechanism is in sharp contrast with wide-bandgap semiconductors (Fig. 5b) in which most of the light energy absorbed reemits as photons after recombination of electron-hole pairs near the bandgap edge. It should also be noted that black phosphorus have received great attention recently because of their excellent photothermal effect across the visible light region [46,47]. However, the challenge for fabrication of large-scale samples and environmental instability limit its practical application for water evaporation [48,49]. An alternative approach relies on encapsulating the black phosphorus devices at early stage during the fabrication [50]. While the experimental work is still scarce and it might be an open field for future development.

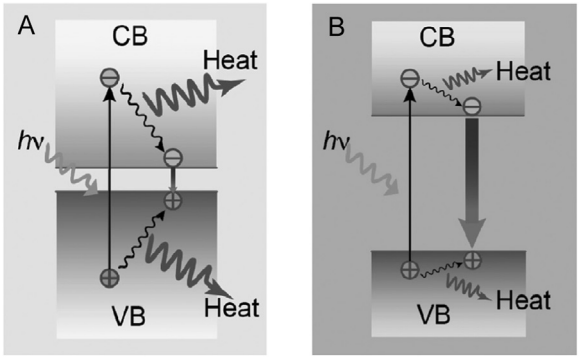

Fig. 5. Illustration of the electron-hole generation and relaxation in A) a narrow-bandgap semiconductor nanocrystal and B) a normal semiconductor. Reproduced with permission [41]. Copyright 2016 Wiley-VCH.

3. Engineering black photothermal sheets for steam generation

3.1. Carbon-based sheets

3.1.1. Single-layer structure

The efficiency of steam generation depends strongly on the absorbers. Carbon-based absorbing materials offer advantages of ultra-high solar absorbance and stability, low cost and easy availability that make them technologically important in solar water evaporation. Various single-layer sheets from pristine carbon systems such as floatable hollow carbon spheres [11], porous graphene [51], flame-treated wood [52], graphene oxide-based aerogels [19], to carbon-loading support systems including reduced graphene oxide within the porous airlaid paper [53], carbon-black-based superhydrophobic gauze [54], microporous cokes in zeolite catalysts [55], porous polymer coated with exfoliated graphite [56] have been developed for vapor generations. Lightweight graphene is a promising candidate because of low molar specific heat, high Debye temperature, outstanding photon-harvesting ability and tunable thermal conductivity by chemical doping. While hydrophobic property and flat nature preclude graphene as a sole component for solar steam generation.

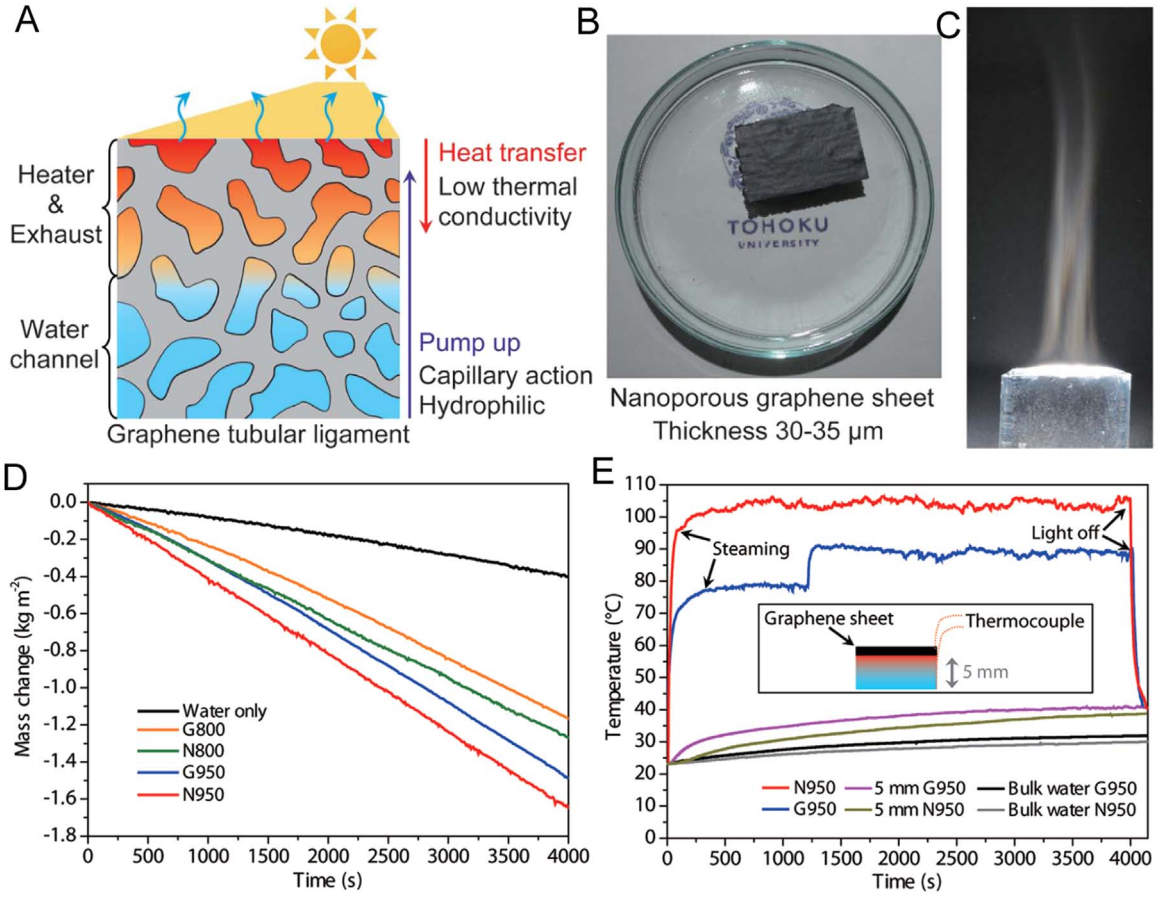

Fig. 6. A) Steam generation using an N-doped porous graphene sheet. B) Optical image of the porous graphene sheet. C) Optical image of steam generation under the concentrated solar illumination. D) Mass loss of water with different samples under one sun illumination. E) The temperature of porous graphene samples versus time under illumination. The solar irradiation close after 4000 s. Reproduced with permission [51]. Copyright 2015 Wiley-VCH.

Porous graphene has thus been functionalized by nitrogen doping or hydrophilic groups for water evaporation [51,57]. Fig. 6**a** shows structure and working principle of the porous graphene steam generator. The porous graphene plays versatile roles in harvesting solar illumination as thermal energy, such as light absorber, heater, water and vapor transport channels etc. The graphene sheets (Fig. 6b) with and without nitrogen doping are synthesized by chemical vapor deposition over nanoporous Ni. In the experiment (Fig. 6c), a single piece of porous graphene achieve solar-to-heat conversion efficiency of 80%. The water evaporation rates are measured to be 1.50 kg m^{-2} h^{-1} for N-doped porous graphene with 1–2 μm pore (N950), and 1.14 kg m^{-2} h^{-1} for N800 with pore size ~ 250 nm, while it is 0.36 kg m^{-2} h^{-1} for water only (Fig. 6d) [51]. The nanometer pore result in better performance than the micrometer pore because of water viscosity slug the water transport to hot regions. Fig. 6e shows temperature rise of the graphene samples and underneath water with light irradiation. It is clear that a temperature jump can be detected for the G950 sample. This is due to bubbles formed at the interface as thermal insulation that prohibits steam escape. To improve the performance, graphene oxide-sodium alginate-carbon nanotube aerogels are prepared to enable solar steam generation [19]. This graphene oxide-aerogel possesses excellent absorption of solar spectrum ~ 92%, good hydrophilicity and porous networks for efficient water supply and vapor channels, and thermal insulating property for heat localization. Hereby, the samples enable ~ 83% energy transfer efficiency under one-sun illumination.

To produce high pressure steam, an flexible-network-structure was fabricated for steam generation [56]. This carbon-loading sheet consists of a porous polymer skeleton coated with exfoliated graphite and artificially-networked 3D veins. The graphite flakes absorb broad band solar illumination and localize solar energy in hot spots in the skeleton structure. The 3D artificial veins transport the fluid to the hot spots for vapor generation. The resulting structure producing steam in the temperature range of 100–156 °C with a pressure of 100–525 kPa that is important for commercial application. As most studies focus on crystalline carbons (graphite [56], graphene and carbon nanotubes [19]), while there is no evidence of their advantages for solar thermal conversion. In fact, a high thermal conductivity of crystalline carbons is unfavorable for heat localization. In contrast with crystalline carbons, amorphous carbons are cheap and abundant, more importantly, they can be facile prepared with tunable textural properties and flexible compositions [52,54]. Cokes from zeolite-catalyzed reactions are easily converted to porous carbons and deposited on a cellulose membrane for steam generation [55]. Due to its interconnected porous structure replicated from zeolite beta and a high content of oxygen in the framework, the carbon derived from the methanol-to-olefin reaction over zeolite beta outperform commercial carbon nanotubes in solar thermal conversion, leading to an efficiency as high as 72% under two suns.

3.1.2. *Duel-layer structure*

A desirable water heating system should simultaneously fulfill requirements of light absorbing, thermally insulating and capillary action. However, it is a challenge to integrate all of the properties into a single-layer structure, and thus duel- or multi-layered sheets are suggested [18,21,58–61]. Chen and co-workers used exfoliated graphite as a top photothermal layer and carbon foam as heat barrier (Fig. 7**a** and b). Under solar irradiation, the duel-layer structure forms an internal hot spot. The fluid wicks to the hot spot, evaporates and releases steam

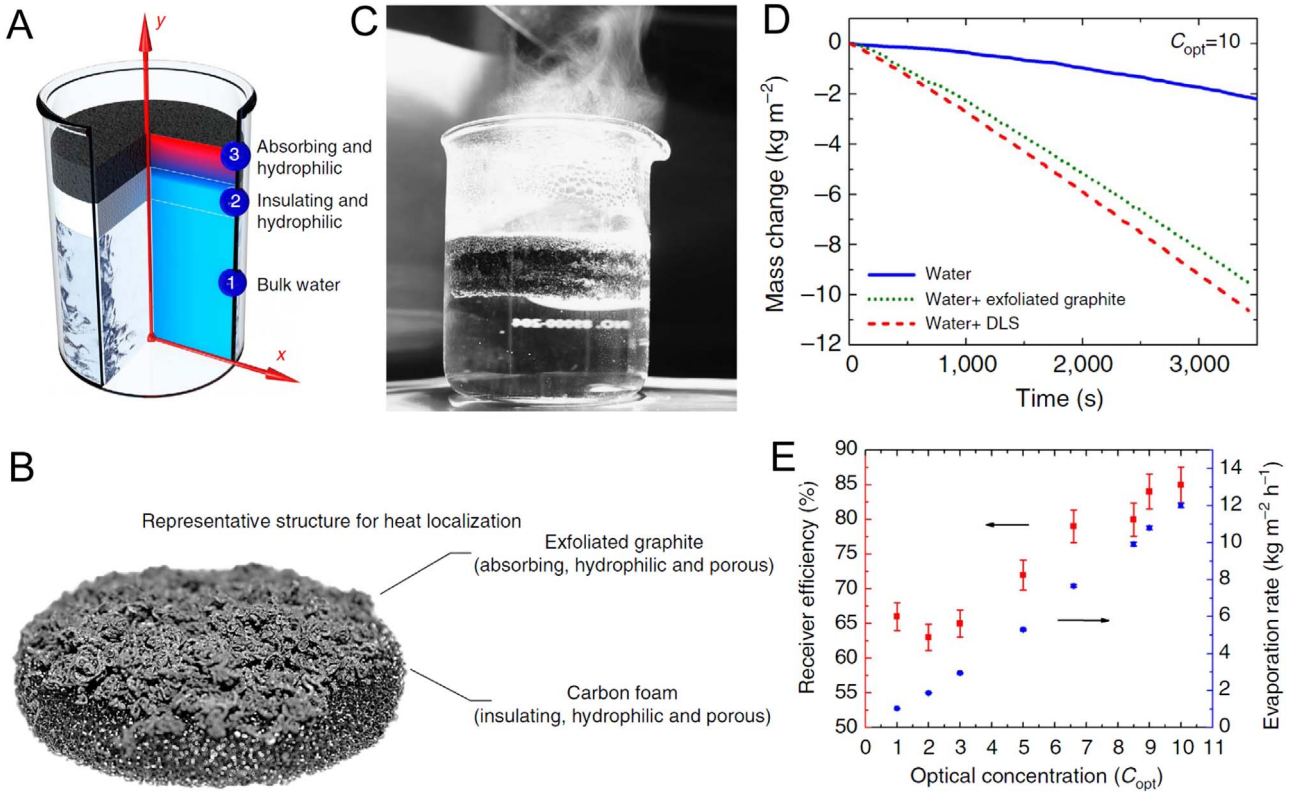

Fig. 7. A) A duel-layer structure for heat localization; the cross section of structure and temperature distribution. B) The duel-layer structure consists of a carbon foam supporting an graphite layer. C) A picture of steam generation. D) Mass change is compared with the case of pure water. E) Solar thermal efficiency of the evaporation process of the duel-layer structure and the corresponding evaporation rate. Reproduced with permission [21]. Copyright 2014 Nature Publishing Group.

from the structure (Fig. 7c) [21]. The evaporation rates with pure water, the duel-layer sheet and the single graphite layer are measured and compared by recording weight loss versus time (Fig. 7d). The duel-layer structure shows the highest evaporation rate and that is 2.4 times higher than pure water, achieving a solar thermal efficiency of 85% at 10 kW/m^2 (Fig. 7e). It is assumed that a higher temperature steam could be anticipated by displacing the carbon foam with a more insulating material, and optimizing thickness and porosity of each layer.

Recently, a bilayered biofoam composed of bacterial nanocellulose (BNC) and reduced graphene oxide (rGO) was introduced for solar steam generation through heat localization at the evaporation surface [59]. Different to normal approaches, the functional biofoam (rGO/BNC:BNC) is fabricated by incorporating GO flakes within the nanocellulose fiber layers during the bacteria-mediated growth of the BNC hydrogel. Owing to its high light absorption, excellent photothermal conversion, heat localization and efficient water transport from bulk to the evaporative surface, this novel structure exhibits a high solar thermal efficiency. The stable evaporation rate reaches ~ 11.8 kg m^{-2} h^{-1} with an efficiency of 83% at a power density of 10 kW/m^2. Moreover, the structure exhibited excellent stability even under vigorous mechanical agitation and harsh chemical conditions. This approach is instructive to prepare cost-effective and scalable heat-localization layers for solar steam generation.

In duel-layer structures, bottom heat barrier and water transport channel are normally combined together, requiring porous structures of heat barrier layers to pump water from bulk water to top photothermal layers. However, overlook in this design is that high porosity of the barrier layer often results in an increased water content, whose heat conductivity is higher than that of the barrier materials, leading to a worse heat barrier performance [18,58,61,62]. To decouple the functions of the heat barrier and water transport, a bi-layered sheet was fabricated with a porous rGO film as a top photothermal layer and solid polystyrene (PS) foam as a heat barrier [18]. The rGO is chosen as light absorber to harvest and convert light to thermal energy as well as water transport channels. The bottom PS layer acts as a thermal barrier to minimize heat transfer to bulk water. The optimized sheet is able to produce water evaporation rate as high as 1.31 kg m^{-2} h^{-1} with light to evaporation conversion efficiency of 83%, which makes it a promising solar steam generator.

3.1.3. *All-in-one structure*

Steam generation under solar irradiation without extra supporting systems will improve the scalability and feasibility of the technology. However, there is intrinsic barriers preventing all of the current designs to achieve this goal. In most of the current designs, the absorbers are always in direct contact with bulk water to ensure the absorbed solar energy can be transferred to bulk water to produce vapors. However, even with heat localization designs, bulk water itself will become an intrinsic thermal conduction path. A significant portion of the absorbed energy would dissipate in the bulk water, evidenced by undesirable temperature increase of bulk water (Fig. 8**a** left). Several all-in-one sheets with spatial separation of the functions are constructed to simultaneously attain suppressed heat loss and efficient water supply [12,13,63].

A composite sheet consisting of a GO film with outstanding photothermal feature sited on a polystyrene foam with low thermal conductivity is proposed to prevent direct contact with bulk water. In addition, a cellulose coating wrapped over the foam function as two-dimensional water transport path via capillary force (Fig. 8a–c) [12,64]. Because the water path is confined to 2D on the surface of thermal insulators, heat loss from absorbers to bulk water is significantly avoided. Fig. 8d–f shows the temperatures of the GO film and the cellulose-wrapped polystyrene foam over time. It can be seen that, by the design of 2D water path, the absorbed energy was highly localized on the GO film. The central temperature of GO film increased from 12.9 °C to 32.1 °C quickly, and stabilized at about 38.8 °C (after

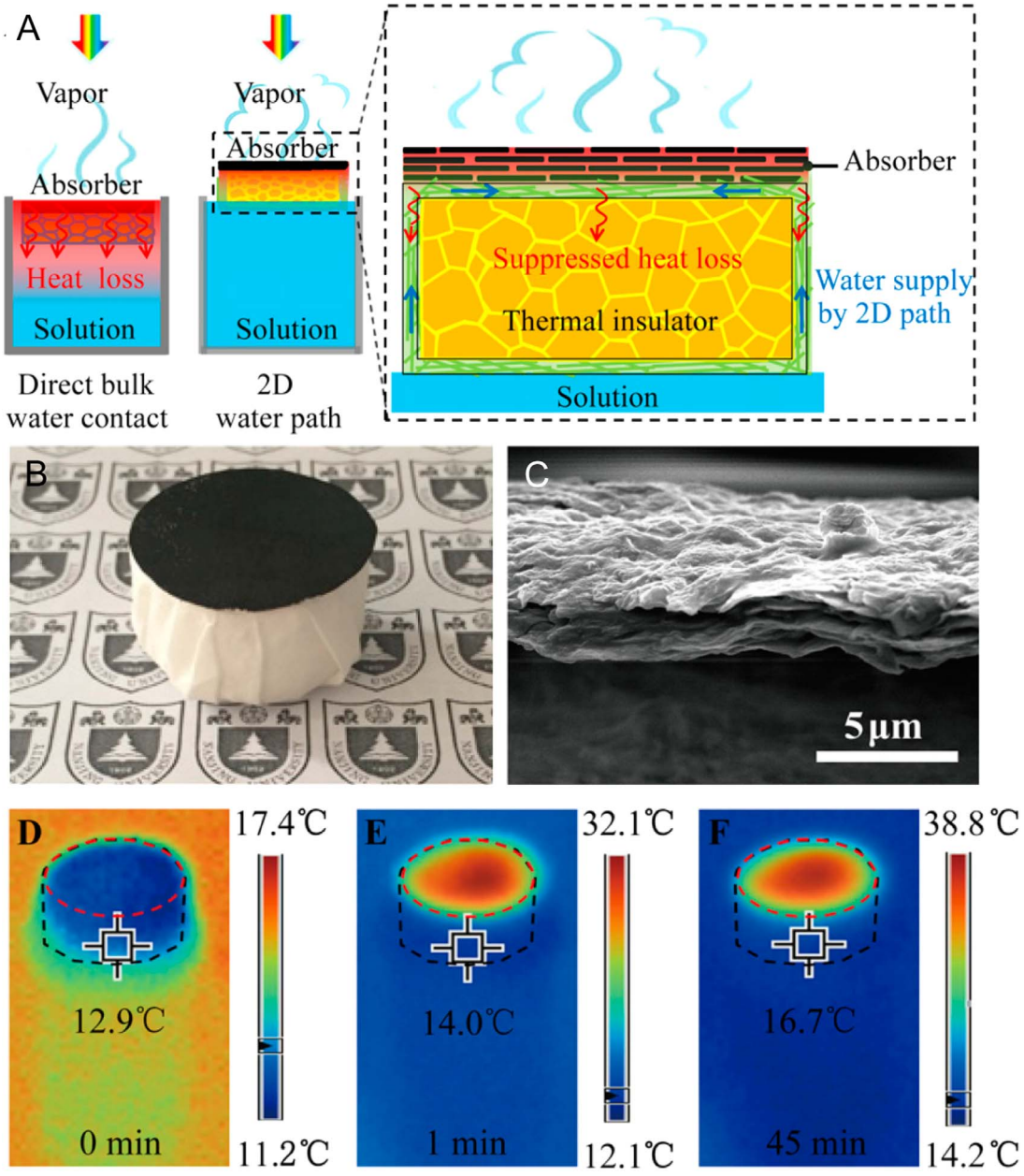

Fig. 8. A) Solar desalination devices with direct water contact (left) and with suppressed heat loss and 2D water supply (right). B) Physical image of the device. C) Cross-section SEM image of the GO film. D–F) Temperatures of the GO film and the cellulose-wrapped polystyrene foam over irradiation time. Reproduced with permission [12]. Copyright 2016 National Academy of Sciences.

45 min). Upon one-sun illumination, this foldable device without optical concentration or thermal supporting systems achieves a conversion efficiency of 80% that provide a portable water solution in remote area.

One challenge of steam generation is to develop easy-to-manufacture and scalable methods to prepare the water evaporator. 3D printing as an efficiency additive manufacturing technology attracts attention [13,65]. An all-in-one evaporator with a concave structure has been fabricated by 3D printing for steam generation. The integrated structure consists of CNT/GO layer, graphene oxide/nanofibrillated cellulose (GO/NFC) layer, and GO/NFC wall (Fig. 9**a** and b) [13]. The CNT/GO layer has an efficient broadband solar absorption and excellent photothermal conversion. Its porous morphology contributes to vapor escape and heat localization. The GO/NFC layer with porous mesh-like structure transport water inside its channels and wick water upward to contiguous CNT/GO layer (Fig. 9c). The porous and hydrophilic GO/NFC support enables effectively water uptake from the bottom owing to capillary effects, forming continuous water transport paths. The air trapped by the GO/NFC wall serve as an effective barrier to alleviate thermal losses to the bulk water. As a result, evaporation rate of the 3D-printed evaporator is ~ 1.25 kg m^{-2} h^{-1}, which is 3.2 times larger than that of pure water (0.39 kg m^{-2} h^{-1}) (Fig. 9d). The solar-to-thermal efficiency reaches up to 85.6% that is one of the highest compared with other reported evaporators. This conceptual design using 3D printing technique offers a new and facile approach to build high-efficiency solar steam devices.

3.2. Plasmonic sheets

3.2.1. Plasmonic metals

Broadband and efficient light absorption is a key step to enable steam generation. Due to strong visible responses overlapping with solar spectrum, plasmonic metal NPs have been extensively studied for

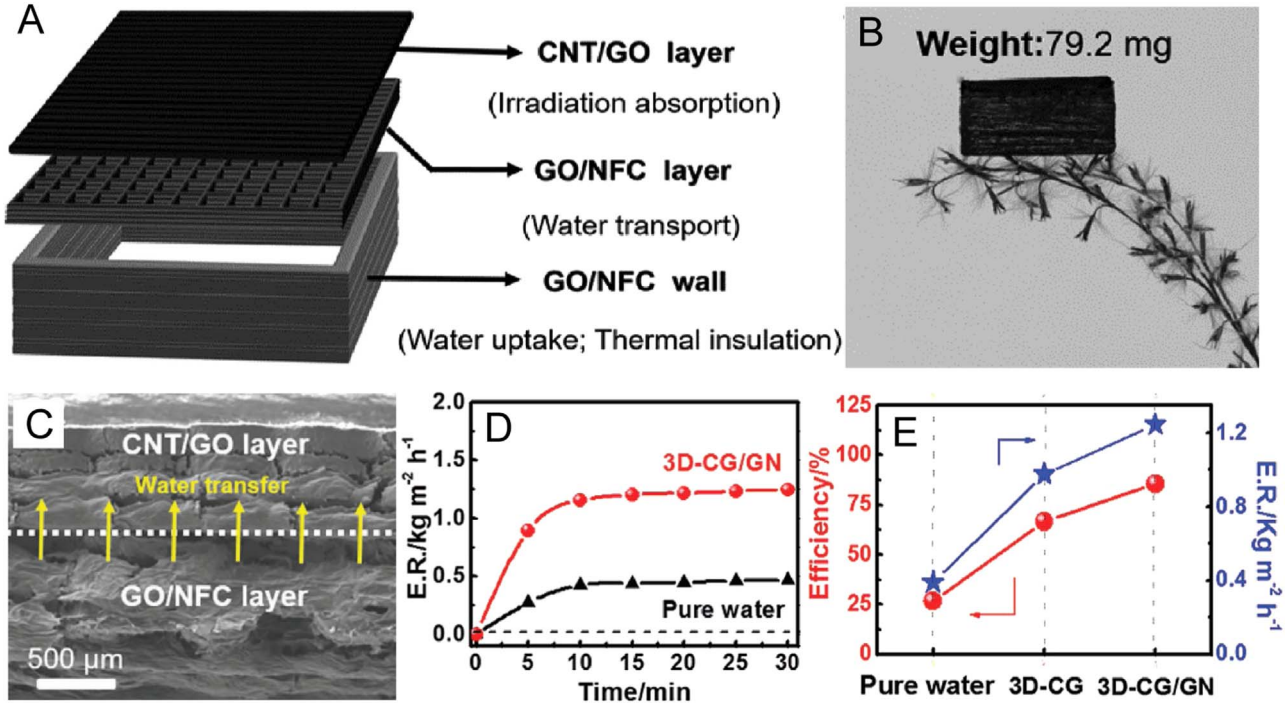

Fig. 9. A) The 3D-printed evaporator consists of CNT/GO layer, GO/CNT layer, and GO/NFC wall. B) Photograph demonstrating the light weight of the evaporator. C) SEM image showing the junction of CNT/GO and GO/NFC layers. D) Dynamic evaporation rate of pure water and the 3D-CG/GN at different times. E) Efficiency and evaporation rate comparison of the pure water, 3D-CG, and 3D-CG/GN samples. Reproduced with permission [13]. Copyright 2017 Wiley-VCH.

vapor generation [66,67]. However, the mechanism of steam generation remains in dispute. Some researchers claimed that evolution of nanobubbles around the NPs migrated to air-water interface release vapor due to their buoyancy [3,7,68]. While others insist that global temperature rising in nanofluid by collective photoheating is the key mechanism for steam generation [8,10,69]. Meanwhile, Wen et al. assume that the steam generation is induced by a highly localized heating in the focal area, while considerable non-uniform temperature distribution exist within the fluid [70]. Specifically to the plasmonic sheets, the plasmon component harvest sunlight and convert it into heat, leading to a hot-zone on the sheet surface that located at gas-liquid interface. Water is uptake into the hot zone for vapor generation through capillary effect of porous materials, and then steam release from the hot-zone to the air.

Inspired by biological systems, a self-assembly procedure has been utilized to prepare Au NP thin films with wide absorption spectrum [71]. The as-prepared films are placed at air-liquid interface with direct contact with bulk water. The plasmonic resonance of Au NPs within the assembled film is used to produce instant, intense and localized heat to drive the evaporation process. This controlled heating of the evaporative surface is similar to the heating of skins through pumping warm blood locally to skin surface or transpiration of water at negative pressures in plants [24,72]. As the skin temperature increases, the evaporation rate also increases to help cool down human body. The steam generation rate is ~ 0.4 mg/s with a 523 nm laser at a power density of 10.18 W/cm^2 after 10 min illumination. Due to the heat loss to the underlying bulk water, photothermal efficiency of the system is only about 44%, but this is still more than twice as high as the efficiency of the suspension system of gold NPs.

The NP structures have inherently narrow absorption bandwidth due to resonant characteristics of surface plasmon excitations. In addition, angle, polarization and wavelength dependence of the plasmonic structures limit the realization of omnidirectional broadband absorber. To attain photothermal conversion using full solar spectrum, adiabatic nanofocusing of surface plasmons is desirable structures. A large-scale, flexible thin-film gold membrane was prepared for the purpose. The resulting membrane has multiscale structures of varying metallic nanoscale gaps (0–200 nm) as well as microscale funnel structures (Fig. 10**a** and b) [25]. The adiabatic nanofocusing of self-aggregated metallic nanowire bundle arrays produces average absorption of 91% at 400–2500 nm and microscale funnel structures lead to average reflection of 7% at 2.5–17 μm. This membrane allows heat localization within few micrometer-thick layer and continuous water supply through micropores. Fig. 10c shows the experimental setup and the side-view infrared images of the black gold membrane under illumination. As a result, vapor generation rate of the structure with three layers of black gold membranes reach 15.59 kg m^{-2} h^{-1} for intensity of 20 kW/m^2 and the thermal conversion efficiency was in the range of 42–57% (Fig. 10d). However, they are impractical for large-scale water evaporation due to their high cost.

3.2.2. *Plasmon-decorated structure*

A retractable sheet floating at air-water interface is preferred for real application and reuse of the system. However, this is not feasible to directly apply assembled plasmonic film since as-prepared gold NP film is fragile and hard to be transferred between various evaporation systems [71]. To address the challenge, various plasmon-decorated sheets including paper-supported Au films [15,72,73], AuNP films sitting on the AAO membrane [74] and Au dimer NPs on a filter paper [75] are optimized for solar water evaporation. A double-layer structure with an Au film acted as the light-to-heat convertor and airlaid paper as supporting and adiabatic layer has been designed (Fig. 11**a** and b) [15]. The paper substrate with increased surface roughness, can produce multiscattering of incident light, yielding high light absorption. Innumerable microscale pores within the paper leverage capillary water flow to the hot zone, leading to rapid replenishment of interfacial steam escape. Compared to the assembled plasmonic sheet, this airlaid-paper-based gold film (PGF) generates localized plasmonic heating only at the solution surface while bulk liquid still remains at low temperature (Fig. 11c and d). Under solar illumination for 15 min with power density of 4.5 kW/m^2, the vapor generation rate is about 1.71 mg/s and the light-to-heat conversion efficiency reaches 77.8%, while conversion

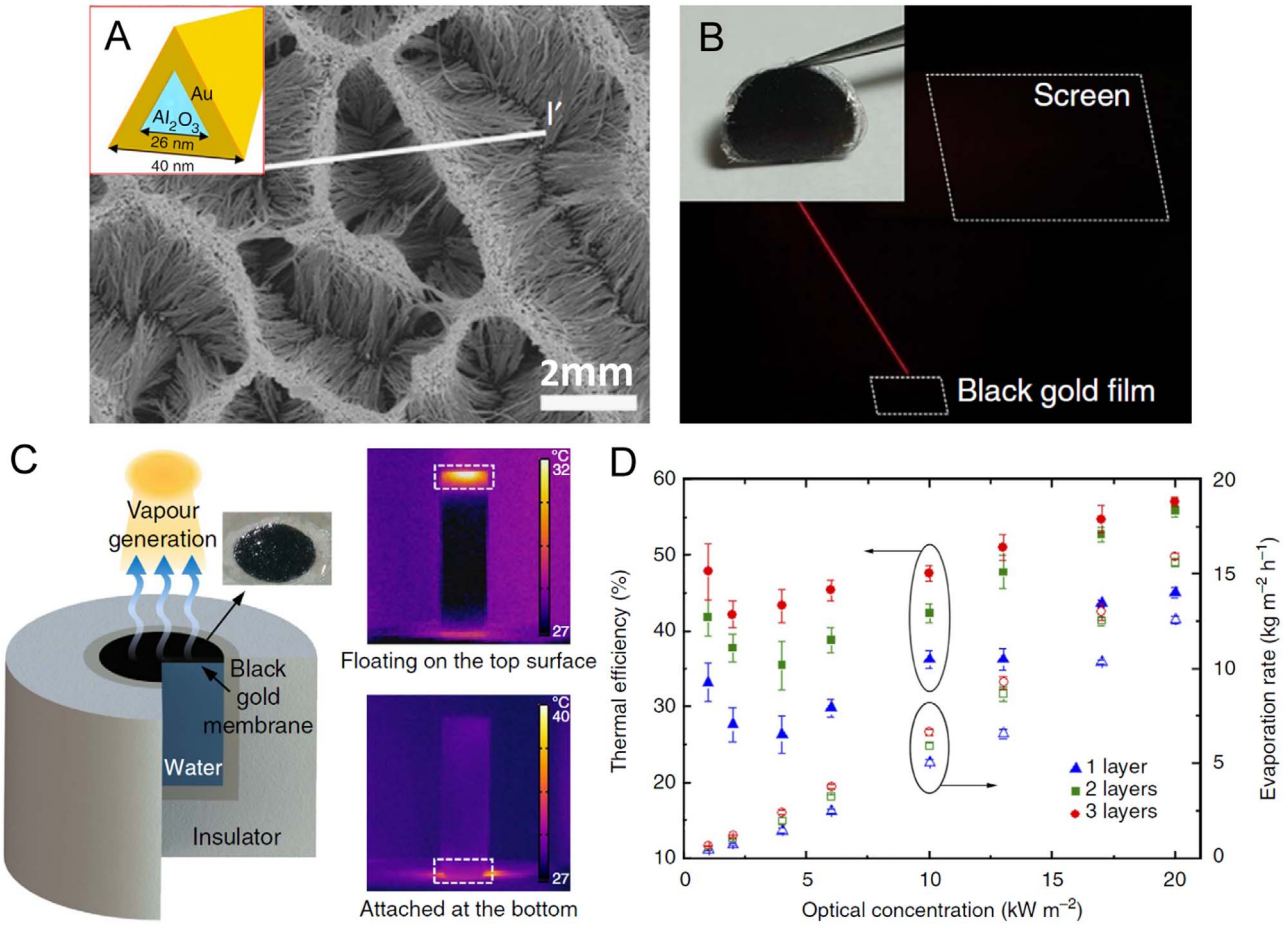

Fig. 10. A) SEM images of the structure, the top ends of collapsed nanowires conglomerate to form ridges. B) Optical photographs displaying the laser beam path reflected by a black gold membrane. C) Experimental setup for vapor generation and a membrane floating on the water surface (inset). Side-view infrared images of the membrane under illumination of 10 kW/m^2 when floating on the top surface of the water cuvette (top) and attached at the bottom of the cuvette (bottom). D) The thermal efficiency and evaporation rate of vapor generation process at varying optical power density. Reproduced with permission [25]. Copyright 2015 Nature Publishing Group.

efficiency of the pristine Au film is only 47.8% (Fig. 11e). Besides, it maintains the high efficiency even when it is recycled multiple times. This floating sheet potentially reduces the cost of extra thermal insulation installment, and further increase the usage of such system.

Light harvesting of metal NP films sitting on AAO membrane is enabled by a limited number of well-defined resonant nanostructures, which are compact-aggregated on bulk optical substrates [72]. To suppress the drawback, physical vapor deposition has been introduced to load Au or Al ions onto the surface of an AAO membrane to prepare efficient, broadband plasmonic absorbers [14,76,77]. Almost all of the ions are deposited onto the membrane surface; however, some of them penetrate into the inner channels of the membrane to form close-packed NPs (Fig. 12**a**–c). There are two key components working together in the structure to attain high performance. Metal NPs with random sizes and distributions enable a high density of hybridized localized surface plasmon resonance (LSPR) to absorb light in a wide wavelength range; nanoporous templates provide an impedance match for efficient reflection reduction and coupling to the optical modes. Therefore, this structure enables an average measured light absorbance of > 96% throughout visible to mid-infrared regimes (Fig. 12d). The steam generation rate with the 3D self-assembled aluminium NPs reaches about 8.9 kg m^{-2} h^{-1} and a photothermal conversion efficiency of 91% under 6-sun illumination (Fig. 12e). Due to its scalable fabrication process and low cost, this solar-steam system could be a portable solution for solar desalination without carbon footprint.

Co-decoration of functional components onto a supporting substrate offers an ideal concept to realize simultaneously solar water evaporation and photocatalytic water purification. Tao et al. designed a bifunctional tri-layer structure that combining an AAO substrate, an Au film for photothermal conversion and TiO_2 islands for photocatalysis [78]. The AAO substrate functions as a supporting layer and a heat insulator. The presence of Au film not only induced vapor generation, but also enhanced photocatalytic reaction because of its near-field enhancement and Schottky junctions contributing to electron-hole separation. The evaporation rate of the TiO_2-AAO sample is 0.24 g/cm^2/h. While the Au-AAO sample and TiO_2-Au-AAO sample showed a much higher evaporation capability, with evaporation rates of 0.51 g/cm^2/h and 0.44 g/cm^2/h, respectively. This reported membrane could be further improved by replacing the Au NPs with other low cost photothermal converters, such as carbon NPs, or by utilizing flexible porous substrates.

3.2.3. *Bulk plasmon-structure*

Plasmonic components integrated with other materials is primarily combined through their assembly on two-dimensional substrates, which limits plasmonically active space to a few nanometers above the substrate. Inclusion of plasmonic elements in bulk material matrixes paves a new way for innovating photothermal sheets [79,80]. It was evidenced that photothermal plasmonic heating generated by Ag NPs dispersed in microporous poly(vinylidene fluoride) PVDF membranes can improve distillation performance. Theoretical analysis demonstrated that the thermal efficiency operated with unloaded membranes is negatively affected by temperature polarization, resulting in a decrease of feed temperature at the membrane surface and, ultimately

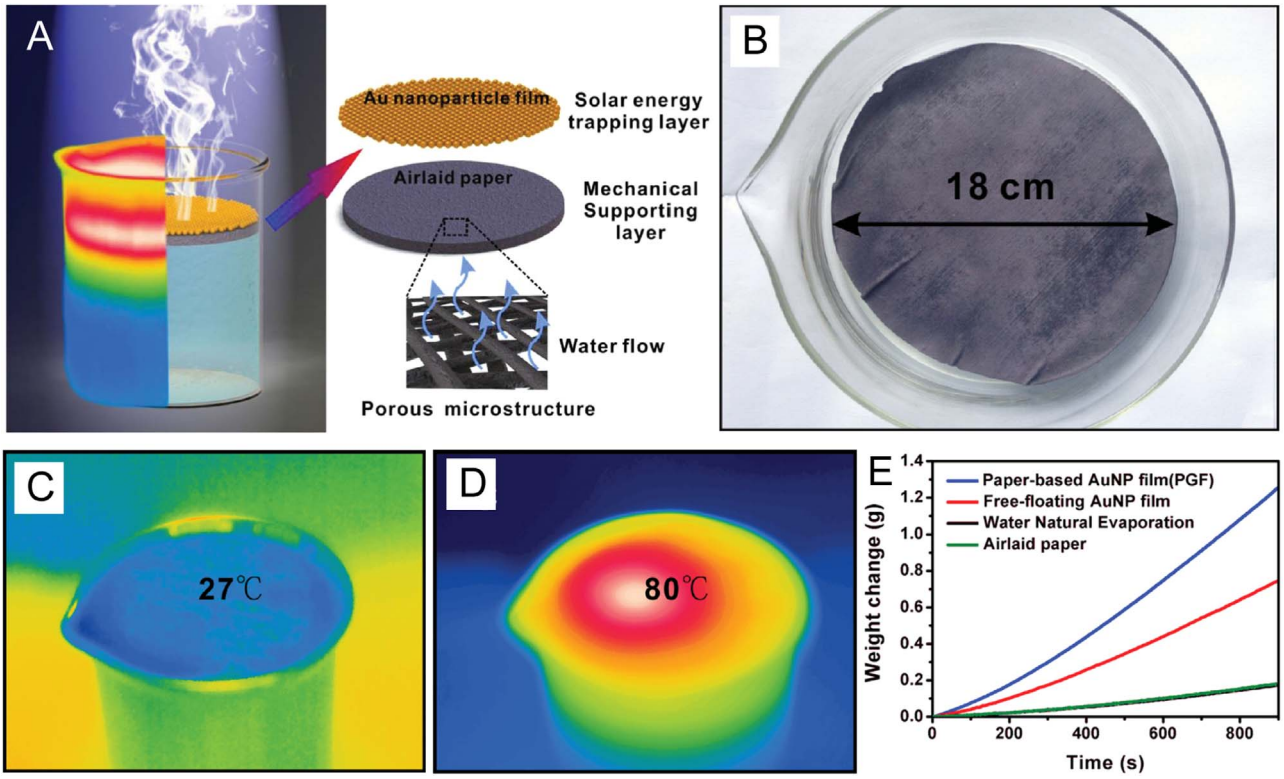

Fig. 11. A) Illustration of the airlaid-paper-based gold NP film (PGF). B) Optical image of PGF with diameter of 18 cm. C) The IR image of PGF before solar illumination. D) The surface temperature distribution of PGF. E) Evaporation weight change of PGF, free-floating Au NP film, water natural evaporation, and airlaid paper under solar power density of 4.5 kW/m^2. Reproduced with permission [15]. Copyright 2015 Wiley-VCH.

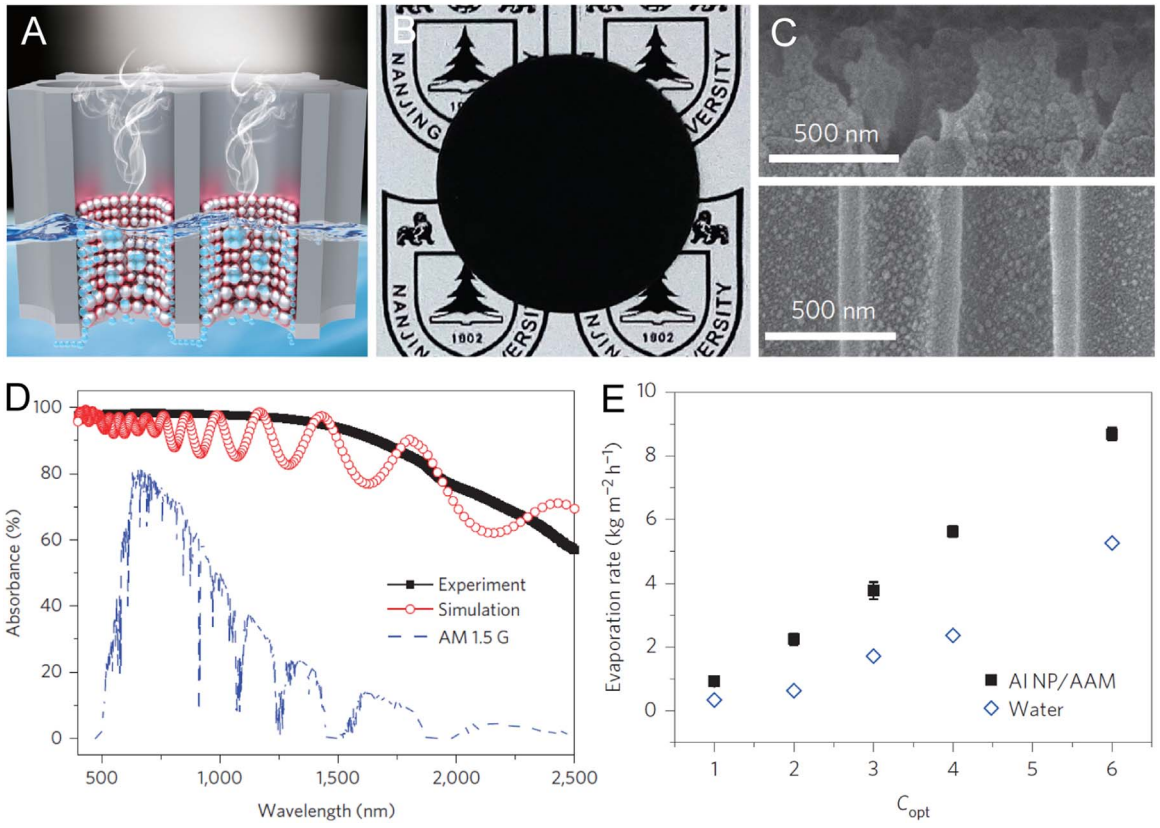

Fig. 12. A) The plasmon-enhanced solar desalination process. B) Optical photographs of the Al NP/AAM structure. C) SEM images of the structure. D) Experimental and simulated absorption of aluminium-based plasmonic absorbers. E) The dependence of the evaporation rate of the Al NP/AAM structure and pure water on optical concentration. Reproduced with permission [14]. Copyright 2016 Nature Publishing Group.

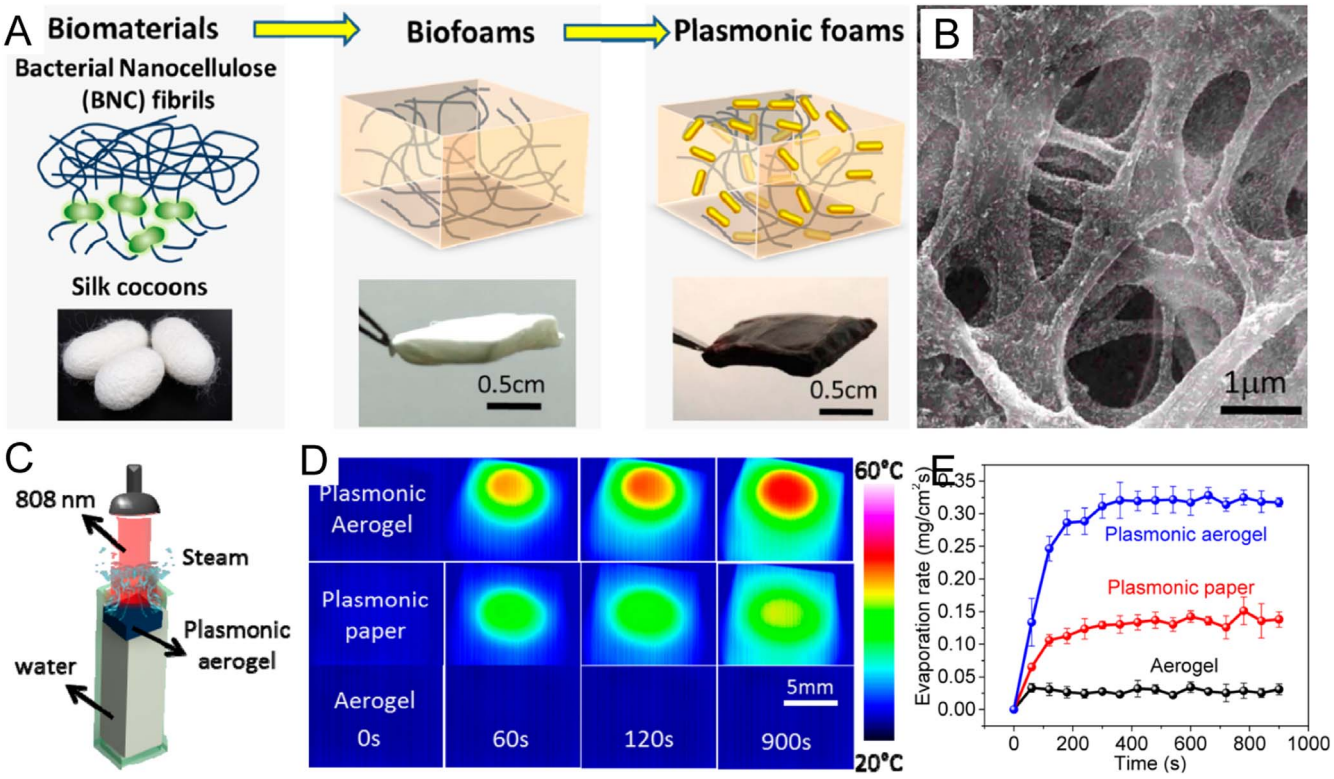

Fig. 13. A) The fabrication process of plasmonic foams. B) SEM images showing the uniform adsorption of Au NRs on silk surface. C) Steam generation using plasmonic aerogel layer suspended at the air-water interface. D) IR images showing the temperature rise of bacterial nanocellulose, plasmonic paper, and plasmonic bacterial nanocellulose aerogel floating on the water surface and E) the instantaneous water evaporation rates. Reproduced with permission [80]. Copyright 2016 American Chemical Society.

reduce driving force to evaporation [79,81]. In contrast, nanoscale thermal hotspots, activated by UV irradiation on loaded Ag NPs in PVDF membranes, reverse temperature profile within the boundary layer neighboring the membrane, leading to an increase of the surface temperature, which is greater more than 23 K with respect to its bulk value. These findings are supported by the experimental evidence of an 11-fold enhancement of the transmembrane flux at the sample with 25% NP concentration.

Singamaneni et al. integrated Au nanorods with biofoams to create bulk plasmonic foams (Fig. 13**a** and b). During their experiments (Fig. 13c), efficiency of 3D plasmonic aerogel and 2D plasmonic paper are compared for steam generation. The temperature rise of pristine bacterial nanocellulose aerogel, plasmonic paper, and plasmonic aerogel suspended on water surface upon irradiation are shown in Fig. 13d. The plasmonic paper or aerogel exhibits significant temperature rise within the first 300 s of irradiation. The evaporation rate of plasmonic aerogel gradually increases to 0.32 mg cm^{-2} s^{-1} and then remains stable during subsequent time. Its steady-state evaporation rate is about 2.3 times higher than that of plasmonic paper (Fig. 13e). This higher evaporation rate is attributed to the higher density of Au nanostructures and multiple scattering of incident light in the 3D aerogel as opposed to the 2D substrate with a monolayer of nanostructures. The thermal conversion efficiency is ~ 76.3% under an 808 nm laser irradiation with a power density of 5.0 W/cm^2 [80]. These results evidence that the bulk plasmon-structure is able to produce desalted water at high thermal efficiency with relatively low energy input, which provides a new basis for innovation of plasmonic photothermal membranes.

3.3. Semiconducting sheets

3.3.1. Black titania

Ideal photothermal materials must have a wide absorption capability and less emissivity that ensure a high photo-to-heat conversion efficiency. In addition, they should be made from abundant elements and can be cost-effectively scaled-up for industrial productions [16]. Titanium is an abundant element and its metal oxides have been intensively studied due to the photoresponse capability, low cost, and thermal stability [82]. However, owing to large bandgap ~ 3.0 eV, intrinsic TiO_2 is white only responds to UV irradiation. In 2011, a hydrogenated black titania with a narrowed bandgap ~ 1.5 eV was reported to boost full spectrum solar absorption [83]. This discovery triggers board scientific interests in black titania materials [84,85]. Black titania is featured by self-structural modifications, e.g. self-doped Ti^{3+}/oxygen vacancy, or incorporation of H-doping. The self-structural modified titania is capable to absorb entire or part of visible-light, resulting in black or colorful appearances (e.g., yellow, blue, green, brown) [86]. Furthermore, the large photothermic effect makes black titania be able to capture solar energy in solar thermal collectors [87]. This is significant to build photothermal sheets.

TiO_x (x < 2) NPs with tunable colors from white to gray to blue-gray to black can be synthesized by magnesium reduction of white P25 nanocrystals followed by removal of excess Mg with aqueous HCl and distilled water [41]. It is found that increasing amounts of Mg decrease oxygen content in TiO_x, which is responsible for gradual increase in light absorption and concomitant darkening of its color with decreasing values of x. The as-synthesized TiO_x NPs are spin-coated onto the surface of a stainless steel mesh followed by surface superhydrophobization to test their performance as a steam evaporator. The black TiO_x efficiently generates water vapor with a thermal efficiency as high as 50% under one-sun irradiation. Ti_2O_3 NP-loaded cellulose membranes has also been tested for vapor generation (Fig. 14**a** and b). The fairly small bandgap ~ 0.1 eV enables the NPs to absorb solar energy in full spectrum range, while the nanoscale feature further enhances the absorption efficiency. With the both advantages, a total absorption capacity of 92.5% was attained (Fig. 14c) that outperform

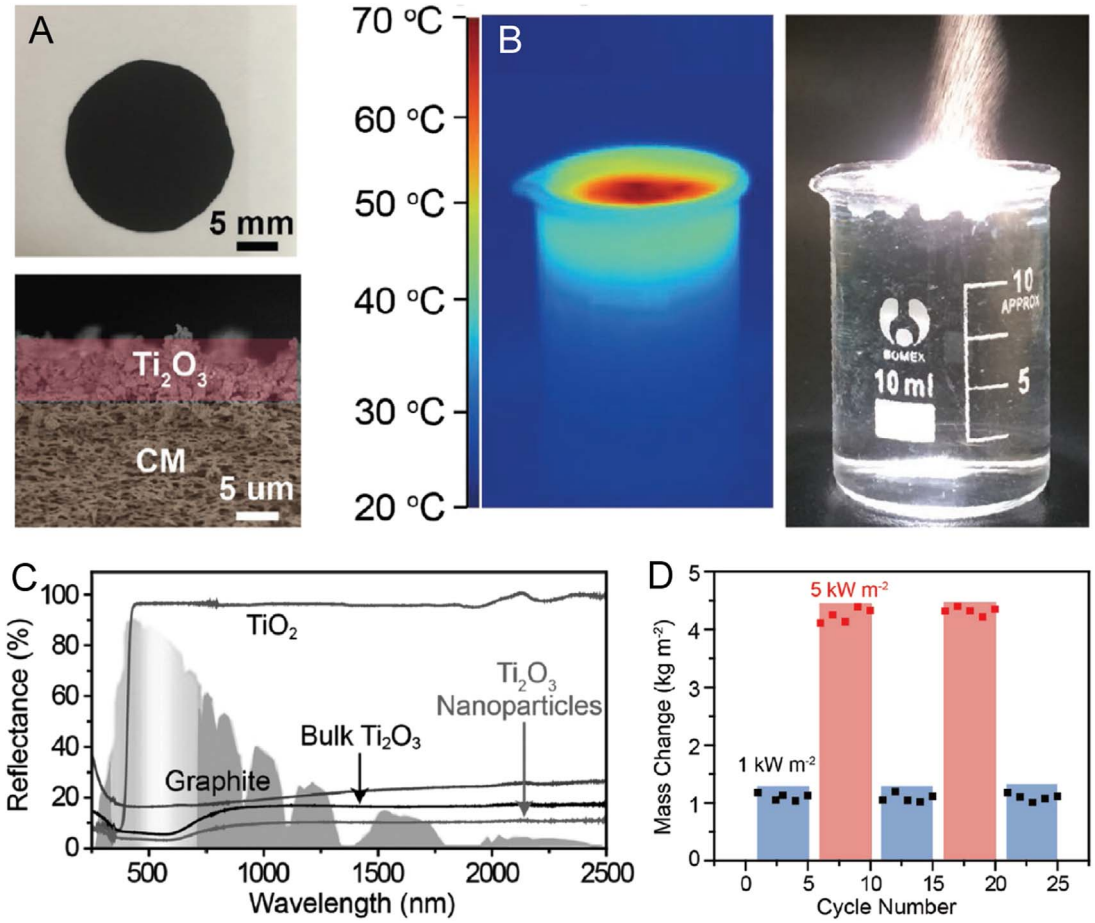

Fig. 14. A) Photograph of the cellulose membrane load with Ti_2O_3 nanoparticle film and SEM cross-section image of the duel-layered structure. B) IR photograph and photograph of the water steam generated under solar illumination of 7 kW/m^2. C) Diffuse reflectance spectra of commercial TiO_2, graphite, commercial Ti_2O_3 powder, and Ti_2O_3 nanoparticles. D) Evaporation cycle performance of the duel-layered structure under different solar simulation light intensities. Reproduced with permission [16]. Copyright 2017 Wiley-VCH.

most of photothermal materials. Evaporation rates of the sheet achieve1.32 kg m^{-2} h^{-1} and 5.03 kg m^{-2} h^{-1} at one and five sun irradiance (Fig. 14d) that are 2.65 and 4.18 times higher than pure water evaporation. This outstanding property offers unique opportunities to develop new solar-thermal systems.

Black titania with a unique nanocage structure has also been synthesized for solar desalination [88]. The nanocage structure increases total absorption due to light trapping effect. Nanocages with interconnected, well-crystallized nanograins accelerate heat transfer from titania to water, and opening mesopores (4–10 nm) facilitate the permeation of water vapor, which help the light-to-heat conversion. The self-floating titania nanocage sheet enables efficiently absorbing solar irradiation, converting it to heat energy, localizing the temperature increase at the air-water interface rather than uniformly heating the bulk water. The light-to-heat conversion could be enhanced as high as 70.9% under one sun illumination. This finding may inspire new black materials with rationally designed structure for superior solar desalination performance.

3.3.2. Copper material

Visible and near-infrared (NIR) light absorbing materials are desirable for real application since both lights compose nearly 40% of total solar energy. NIR responsive photothermal materials are attracting interest since the wavelength of NIR is larger than most water drops in cloud and thus avoid the blocking of cloud much easier than visible light. As a result, energy harvesting from NIR light is promising for steam generation. Au nanostructures are being the most NIR responsive agent with excellent photothermal property [89,90]. While practical applications of the structures are limited due to its high price and poor photostability after a long period of irradiation. To overcome the issue, new types of light-to-heat nanomaterials including copper phosphate and sulfides, as well as other copper compounds are developed for solar evaporation [42,44,91,92]. These compounds show strong vis-NIR absorption due to d-d transition of Cu^{2+}.

Hierarchical microstructured copper phosphate (HCuPO) has been designed based on d-d transition of 3d electrons in Cu^{2+} and fabricated via a solvothermal method (Fig. 15**a**). A strong vis-NIR absorption with maximum at 808 nm was observed for as-prepared HCuPO (Fig. 15b). Upon irradiation of 808 nm NIR laser light, the HCuPO generated heat with a light-to-heat converting efficiency of 41.8% [91]. The reason of this is assigned to a probability of nonradiative relaxation, which released the energy in form of heat, happened to the excited 3d electrons of Cu^{2+} (Fig. 15c). This is quite different from the surface-plasmon mechanism of Cu-based photothermal materials. By adding HCuPO into polydimethylsiloxane (PDMS), HCuPO-PDMS sheets are fabricated to assist water evaporation. Due to intrinsic hydrophobicity of PDMS matrix, the sheets can float on water surface and the heat generated by HCuPO is confined within water-air interface region. Under 808 nm laser irradiation with power density of 1–2 kW/m^2, a sharp temperature gradient and rapid increase of surface temperature are observed (Fig. 15d). Water evaporation rate is measured to be 1.13–1.85 kg m^{-2} h^{-1} for porous floating HCuPO-PDMS, which is 2.2–3.6 times of that of the salt water without HCuPO (Fig. 15e). Copper sulfides has recently demonstrated as photothermal materials exhibiting a significant photothermal efficiency ~ 56.7% due to its strong near-infrared localized surface plasmon resonance property and

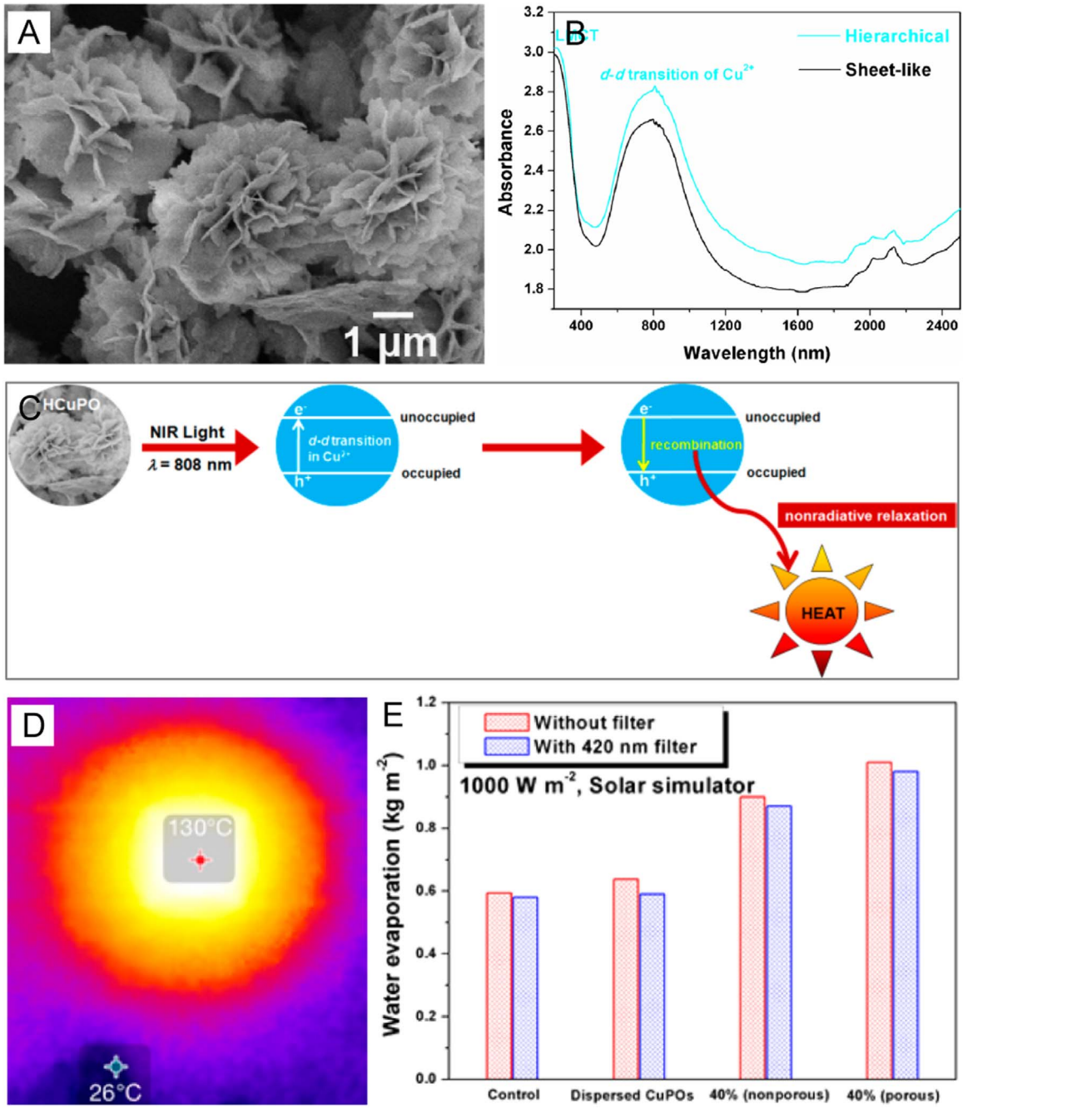

Fig. 15. A) A SEM image of HCuPO. B) UV–vis–NIR diffuse reflection spectra of copper phosphate powder with different morphology. C) light-to-heat converting mechanism of HCuPO. D) IR images of nonporous HCuPO-PDMS composite sheets with 40% HCuPO percentage under 808 nm laser illumination of 2 kW/m^2 for 5 min. E) Weight loss profiles of salt water with and without HCuPO-PDMS sheets. Reproduced with permission [91]. Copyright 2017 American Chemical Society.

the supramolecular free radical [93,94]. Wang et al. employed a shape-controlling synthesis approach to prepare different shapes of Cu_7S_4 nanocrystals [42]. Because of its excellent photothermal performance in NIR region, the nanocrystal film placed on water surface exhibits a 77.1% energy conversion efficiency under an infrared lamp for 15 min at a power density of 1 kW/m^2.

To reduce the cost of optical concentrator, a floating solar receiver with three key components was designed (Fig. 16**a**): 1) A transparent bubble jacket wraps on the light absorber for reducing the convective heat loss. 2) A cermet-coated copper substrate acts as selective absorber with high solar absorbance and low thermal emissivity. 3) A polystyrene foam functions as support for floating entire structure on water as well as heat insulation. There is a fabric wick hiding in the foam center to tunnel water through the foam from the underlying water [92]. To obtain high steam temperature, evaporative slots that are smaller than absorbing area were cut into selective absorber for thermal concentration. As a result, the thermal concentration is ratio of evaporation area to solar absorption area. In conventional steam system, one sun illumination is not enough to sustain the heat losses, leading to an equilibrium temperature of 100 °C for evaporation (Fig. 16b). While by this special device structure (Fig. 16c), a steam temperature of 100 °C is achieved under one sun irradiation when the thermal concentration was about 200. This one sun, ambient vapor generation system is low cost and sufficient to enhance the water evaporation rate or steam temperature by optimizing the evaporative slots in the light absorber.

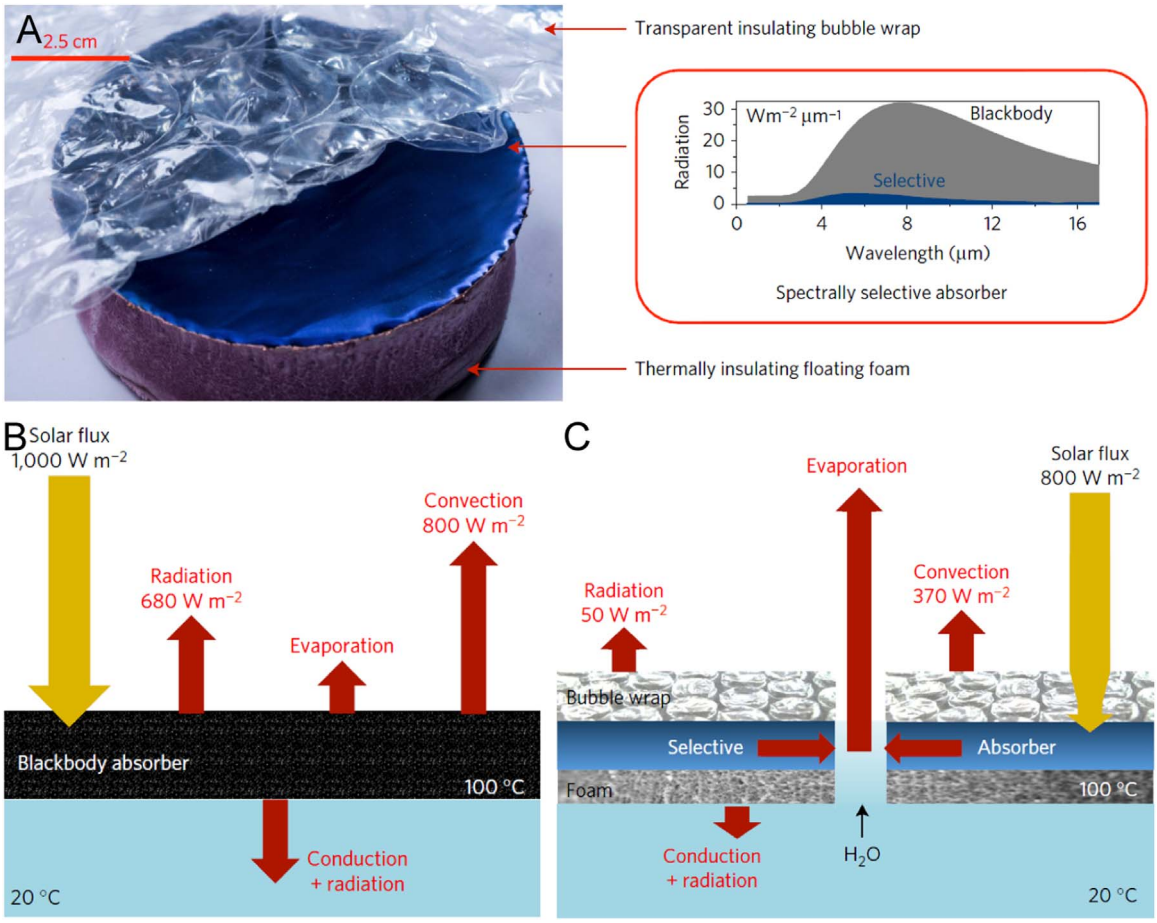

Fig. 16. Operating principles of steam generation at one sun. A) Photograph of the ambient steam generator composed of a spectrally selective coating on copper to suppress radiative losses and to thermally concentrate heat to the evaporation region. The inset compares thermal radiative losses at 100 °C from a blackbody and the spectrally selective absorber. B) Energy balance and heat transfer diagram for a blackbody solar receiver operating at 100 °C. The one sun illumination is not enough to sustain the heat losses, and an equilibrium temperature cannot be reached. C) Energy balance in the developed one-sun ambient steam generator. Reproduced with permission [92]. Copyright 2016 Nature Publishing Group.

3.3.3. Polypyrrole (organic material)

Steam generation is a surface process, in which water molecules in thin air-water interface at liquid side. Driven by their high energy state under heat localization, the water molecules are transported into vapor phase. The surface hydrophobicity, given generally by alkyl or fluoroalkyl group surface modification is prerequisite to a self-floating sheet at air-water interface. While in practical application, the induced chemical reaction from exposure to strong light or highly oxidative chemicals in air and water often results in deterioration of surface hydrophobicity, leading to hydrophilic wettability of the materials. Therefore, a hydrophobicity self-healing photothermal material that can heal or recover its hydrophobicity autonomously upon degradation is desirable for practical application.

In response to this requirement, Wang's group constructed a self-healing hydrophobic photothermal sheet (Fig. 17**a**). The system is based on a polypyrrole (PPy) coating on stainless steel (SS) meshes with hydrophobic treatment by fluoroalkylsilane modification [95]. The organic material PPy acts as photothermal material, while the stainless steel is the scaffold. The hydrophobic modification contributed to the material floating on water surface. Upon one sun illumination, the interfacial water temperature in presence of the sheet increase immediately (Fig. 17b). The steam generation rate reaches $0.92\ kg\ m^{-2}\ h^{-1}$ for 2 h via 2.6 mm-thick PPy with 500 mesh (Fig. 17c). The conversion efficiency of the system is ~ 58% that stands favorably against the case without the sheet, whose conversion efficiency is only 24%. Beside, upon loss of their hydrophobicity, the membranes can be autonomously restored their hydrophobicity under light irradiation via self-migration of the fluoroalkylsilane. This study presents a new avenue for the design of next-generation solar heating system and thus potentially contributes to the global effort in actual applications.

PPy materials are attractive photothermal agents owing to their wide absorption spectrum and excellent photothermal properties. This material is a traditional thermal desalination material, and porous polypropylene membranes have been used as thermal desalination membrane for decades [96]. PPy thin film coating on polypropylene mesh has thus been proposed as desalination membranes to vaporize seawater or brackish water [97]. In addition to its outstanding efficiency and stability, PPy also exhibits good biocompatibility and long-term cytotoxicity with low cost as compared to metal nanoparticles and carbon materials. Moreover, current technology allows PPy thin film to tightly coat on a variety of substrates regardless of their curvature and conductivity. With coating ~ 300 nm PPy thin film on polypropylene mesh, the solar steam generation efficiency is measured to be 72%, which is higher than that of the commercialized solar stills with typical efficiencies from 24% to 45%. This technique opens doors to next generation of thermal desalination membrane utilizing solar energy.

4. Summary and prospects

This work addresses physical understanding and experimental advances in development of black photothermal sheets, and illustrates their key features for water evaporation. Particularly, we focus our discussion on three essential forms of black sheets: carbon-based sheets,

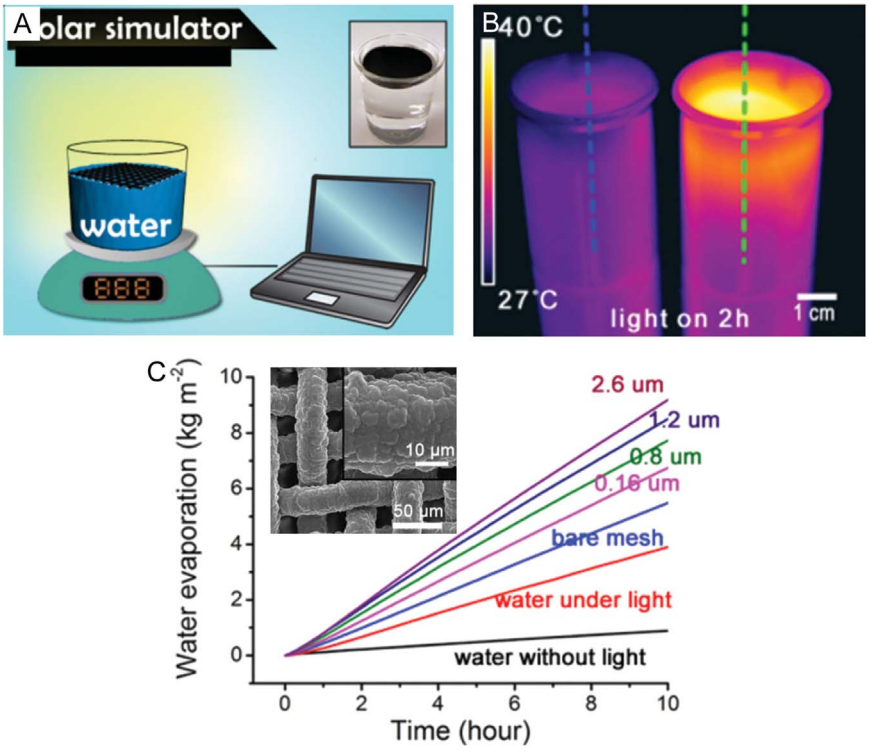

Fig. 17. A) The water-evaporation setup with PPy-coated SS mesh floating on the water surface. B) IR images of water beakers without light and with light irradiation for 2 h. C) Time course of water evaporation under various conditions. Pink, green, purple, and brown: water with floating SS meshes with different PPy coating thicknesses. The inset shows the magnified view of the knitting wire surfaces. Reproduced with permission [43]. Copyright 2015 Wiley-VCH.

plasmonic sheets as well as semiconducting sheets. Many intriguing black materials have been selected to demonstrate the conceptual development, which includes amorphous carbon, graphite or graphene, carbon nanotubes; plasmonic metals and plasmon-decorated supporting material; black titana, copper sulfide or phosphate, PPys, etc. Three key factors yielding remarkable photothermal performance have been identified to the state-of-the-art design of the photothermal-sheets: i) Black materials with broadband absorption and high photothermal properties can harvest more sunlight and then convert the light energy into heat. ii) An insulation layer between the absorber and the bulk water reduce heat loss from the absorber to the underlying water, so that the heat can be localized in the absorber region for evaporation. iii) Hydrophobicity is prerequisite to a self-floating sheet, while a hydrophilic bottom layer with porous and/or channel networks is necessary for negative transpiration of water. Although this research area is at initial stage, obvious achievements have been achieved in steam generation by using black photothermal sheets. The major experiments demonstrate a high efficient converting solar energy into heat (e.g. carbon-sheets $\eta_{th} =$ 70–85%, plasmonic sheets $\eta_{th} =$ 40–88% and semiconducting sheets $\eta_{th} =$ 50–77%). Further improvement in steam output can be expected by optimizing the photothermal nanomaterials, device structures as well as the quality of water, such as tap water, waste water or sea water, etc. Multifunctional systems also can be developed not only for steam generation, but also for water purification and/or desalination.

Despite the current achievements and promising prospects, some challenges in either physical mechanism or empirical aspects are still need further investigation. Future effort are likely to focus on clarifying the mechanisms in detail to identify the key factor for solar water evaporation. In addition to basic understanding of the behind physics, novel concept and structure designs, controlled synthesis and assembly of black nanomaterials are interesting aspects to be explored. Manufacturing or integration processes such as physical vapor deposition, wet chemical synthesis and vacuum-filtration assembly are required to meet the technique goals. Rational design of the experiment and proper use of numerical models would be helpful to provide insights into the mechanism of vapor generation [70,98–100]. The unified models that describe complex interactions between solar light, photothermal material and liquid media are urgently to be developed. Since there is much scope for black photothermal sheets, we believe that this black-photothermal dream could one day come true and scalable for commercial applications.

Notes

The authors declare no competing financial interest.

Acknowledgements

This work has been supported with grants from the National Natural Science Foundation of China (51576002) and the Norwegian Research Council-Independent Projects-Mathematics, Physical Science and Technology (FRINATEK) Programme (231416/F20).

References

[1] M.A. Shannon, P.W. Bohn, M. Elimelech, J.G. Georgiadis, B.J. Marinas, A.M. Mayes, Nature 452 (2008) 301–310.
[2] M. Elimelech, W.A. Phillip, Science 333 (2011) 712–717.
[3] O. Neumann, C. Feronti, A.D. Neumann, A. Dong, K. Schell, B. Lu, E. Kim, M. Quinn, S. Thompson, N. Grady, P. Nordlander, M. Oden, N.J. Halas, Proc. Natl. Acad. Sci. USA 110 (2013) 11677–11681.
[4] M. Thirugnanasambandam, S. Iniyan, R. Goic, Renew. Sustain. Energy Rev. 14 (2010) 312–322.
[5] M.J. Montes, A. Abánades, J.M. Martínez-Val, Sol. Energy 83 (2009) 679–689.
[6] S. Al-Kharabsheh, D.Y. Goswami, Sol. Energy 75 (2003) 395–401.
[7] O. Neumann, A.S. Urban, J. Day, S. Lal, P. Nordlander, N.J. Halas, ACS Nano 7 (2013) 42–49.
[8] H.H. Richardson, M.T. Carlson, P.J. Tandler, P. Hernandez, A.O. Govorov, Nano Lett. 9 (2009) 1139–1146.
[9] M. Gao, P.K.N. Connor, G.W. Ho, Energy Environ. Sci. 9 (2016) 3151–3160.
[10] N.J. Hogan, A.S. Urban, C. Ayala-Orozco, A. Pimpinelli, P. Nordlander, N.J. Halas, Nano Lett. 14 (2014) 4640–4645.
[11] J. Zhou, Z. Sun, M. Chen, J. Wang, W. Qiao, D. Long, L. Ling, Adv. Funct. Mater. 26 (2016) 5368–5375.
[12] X. Li, W. Xu, M. Tang, L. Zhou, B. Zhu, S. Zhu, J. Zhu, Proc. Natl. Acad. Sci. USA 113 (2016) 13953–13958.
[13] Y. Li, T. Gao, Z. Yang, C. Chen, W. Luo, J. Song, E. Hitz, C. Jia, Y. Zhou, B. Liu, B. Yang, L. Hu, Adv. Mater. (2017))1700981.

[14] L. Zhou, Y. Tan, J. Wang, W. Xu, Y. Yuan, W. Cai, S. Zhu, J. Zhu, Nat. Photonics 10 (2016) 393–398.
[15] Y. Liu, S. Yu, R. Feng, A. Bernard, Y. Liu, Y. Zhang, H. Duan, W. Shang, P. Tao, C. Song, T. Deng, Adv. Mater. 27 (2015) 2768–2774.
[16] J. Wang, Y. Li, L. Deng, N. Wei, Y. Weng, S. Dong, D. Qi, J. Qiu, X. Chen, T. Wu, Adv. Mater. 29 (2017) 1603730.
[17] W. Shang, T. Deng, Nat. Energy 1 (2016) 16133.
[18] L. Shi, Y. Wang, L. Zhang, P. Wang, J. Mater. Chem. A 5 (2017) 16212–16219.
[19] X. Hu, W. Xu, L. Zhou, Y. Tan, Y. Wang, S. Zhu, J. Zhu, Adv. Mater. 29 (2017), http://dx.doi.org/10.1002/adma.201604031.
[20] F.M. Canbazoglu, B. Fan, A. Kargar, K. Vemuri, P.R. Bandaru, AIP Adv. 6 (2016) 085218.
[21] H. Ghasemi, G. Ni, A.M. Marconnet, J. Loomis, S. Yerci, N. Miljkovic, G. Chen, Nat. Commun. 5 (2014) 4449.
[22] T.D. Wheeler, A.D. Stroock, Nature 455 (2008) 208–212.
[23] R. Xiao, S.C. Maroo, E.N. Wang, Appl. Phys. Lett. 102 (2013) 123103.
[24] A.D. Stroock, V.V. Pagay, M.A. Zwieniecki, N. Michele Holbrook, Annu. Rev. Fluid Mech. 46 (2014) 615–642.
[25] K. Bae, G. Kang, S.K. Cho, W. Park, K. Kim, W.J. Padilla, Nat. Commun. 6 (2015) 10103.
[26] W.F. Bogaerts, C.M. Lampert, J. Mater. Sci. 18 (1983) 2847–2875.
[27] H. Dotan, O. Kfir, E. Sharlin, O. Blank, M. Gross, I. Dumchin, G. Ankonina, A. Rothschild, Nat. Mater. 12 (2013) 158–164.
[28] A.O. Govorov, H.H. Richardson, Nano Today 2 (2007) 30–38.
[29] Q. Zhao, T. Fan, J. Ding, D. Zhang, Q. Guo, M. Kamada, Carbon 49 (2011) 877–883.
[30] E.A. Taft, H.R. Philipp, Phys. Rev. 138 (1965) A197–A202.
[31] F.J. García-Vidal, J.M. Pitarke, J.B. Pendry, Phys. Rev. Lett. 78 (1997) 4289–4292.
[32] K. Mizuno, J. Ishii, H. Kishida, Y. Hayamizu, S. Yasuda, D.N. Futaba, M. Yumura, K. Hata, Proc. Natl. Acad. Sci. USA 106 (2009) 6044–6047.
[33] S. Thongrattanasiri, F.H. Koppens, F.J. Garcia de Abajo, Phys. Rev. Lett. 108 (2012) 047401.
[34] A.M. Kolpak, J.C. Grossman, Nano Lett. 11 (2011) 3156–3162.
[35] A.V. Dudchenko, C. Chen, A. Cardenas, J. Rolf, D. Jassby, Nat. Nanotechnol. 12 (2017) 557–563.
[36] X. Zheng, L. Zhang, Energy Environ. Sci. 9 (2016) 2511–2532.
[37] M.L. Brongersma, N.J. Halas, P. Nordlander, Nat. Nanotechnol. 10 (2015) 25–34.
[38] G. Liu, K. Du, J. Xu, G. Chen, M. Gu, C. Yang, K. Wang, H. Jakobsen, J. Mater. Chem. A 5 (2017) 4233–4253.
[39] T. Liu, Y. Li, Nat. Photonics 10 (2016) 361–362.
[40] C. Jia, X. Li, N. Xin, Y. Gong, J. Guan, L. Meng, S. Meng, X. Guo, Adv. Energy Mater. 6 (2016) 1600431.
[41] M. Ye, J. Jia, Z. Wu, C. Qian, R. Chen, P.G. O'Brien, W. Sun, Y. Dong, G.A. Ozin, Adv. Energy Mater. 7 (2017) 1601811.
[42] C. Zhang, C. Yan, Z. Xue, W. Yu, Y. Xie, T. Wang, Small 12 (2016) 5320–5328.
[43] L. Zhang, B. Tang, J. Wu, R. Li, P. Wang, Adv. Mater. 27 (2015) 4889–4894.
[44] Q. Tian, F. Jiang, R. Zou, Q. Liu, Z. Chen, M. Zhu, S. Yang, J. Wang, J. Wang, J. Hu, ACS Nano 5 (2011) 9761–9771.
[45] M. Umlauff, J. Hoffmann, H. Kalt, W. Langbein, J.M. Hvam, M. Scholl, J. Söllner, M. Heuken, B. Jobst, D. Hommel, Phys. Rev. B 57 (1998) 1390–1393.
[46] Z. Sun, H. Xie, S. Tang, X.F. Yu, Z. Guo, J. Shao, H. Zhang, H. Huang, H. Wang, P.K. Chu, Angew. Chem. Int. Ed. Engl. 54 (2015) 11526–11530.
[47] J. Shao, H. Xie, H. Huang, Z. Li, Z. Sun, Y. Xu, Q. Xiao, X.F. Yu, Y. Zhao, H. Zhang, H. Wang, P.K. Chu, Nat. Commun. 7 (2016) 12967.
[48] A. Castellanos-Gomez, J. Phys. Chem. Lett. 6 (2015) 4280–4291.
[49] G. Abellan, S. Wild, V. Lloret, N. Scheuschner, R. Gillen, U. Mundloch, J. Maultzsch, M. Varela, F. Hauke, A. Hirsch, J. Am. Chem. Soc. 139 (2017) 10432–10440.
[50] Y. Zhao, H. Wang, H. Huang, Q. Xiao, Y. Xu, Z. Guo, H. Xie, J. Shao, Z. Sun, W. Han, X.F. Yu, P. Li, P.K. Chu, Angew. Chem. Int. Ed. Engl. 55 (2016) 5003–5007.
[51] Y. Ito, Y. Tanabe, J. Han, T. Fujita, K. Tanigaki, M. Chen, Adv. Mater. 27 (2015) 4302–4307.
[52] G. Xue, K. Liu, Q. Chen, P. Yang, J. Li, T. Ding, J. Duan, B. Qi, J. Zhou, ACS Appl. Mater. Interfaces 9 (2017) 15052–15057.
[53] J. Lou, Y. Liu, Z. Wang, D. Zhao, C. Song, J. Wu, N. Dasgupta, W. Zhang, D. Zhang, P. Tao, W. Shang, T. Deng, ACS Appl. Mater. Interfaces 8 (2016) 14628–14636.
[54] Y. Liu, J. Chen, D. Guo, M. Cao, L. Jiang, ACS Appl. Mater. Interfaces 7 (2015) 13645–13652.
[55] J. Wang, Z. Liu, X. Dong, C.-E. Hsiung, Y. Zhu, L. Liu, Y. Han, J. Mater. Chem. A 5 (2017) 6860–6865.
[56] S.M. Sajadi, N. Farokhnia, P. Irajizad, M. Hasnain, H. Ghasemi, J. Mater. Chem. A 4 (2016) 4700–4705.
[57] J. Yang, Y. Pang, W. Huang, S.K. Shaw, J. Schiffbauer, M.A. Pillers, X. Mu, S. Luo, T. Zhang, Y. Huang, G. Li, S. Ptasinska, M. Lieberman, T. Luo, ACS Nano 11 (2017) 5510–5518.
[58] Z. Liu, H. Song, D. Ji, C. Li, A. Cheney, Y. Liu, N. Zhang, X. Zeng, B. Chen, J. Gao, Y. Li, X. Liu, D. Aga, S. Jiang, Z. Yu, Q. Gan, Glob. Chall. 1 (2017) 1600003.
[59] Q. Jiang, L. Tian, K.K. Liu, S. Tadepalli, R. Raliya, P. Biswas, R.R. Naik, S. Singamaneni, Adv. Mater. 28 (2016) 9400–9407.
[60] G. Wang, Y. Fu, X. Ma, W. Pi, D. Liu, X. Wang, Carbon 114 (2017) 117–124.
[61] N. Xu, X. Hu, W. Xu, X. Li, L. Zhou, S. Zhu, J. Zhu, Adv. Mater. (2017) 1606762.
[62] X. Li, R. Lin, G. Ni, N. Xu, X. Hu, B. Zhu, G. Lv, J. Li, S. Zhu, J. Zhu, Natl. Sci. Rev. (2017), http://dx.doi.org/10.1093/nsr/nwx051.
[63] P. Zhang, J. Li, L. Lv, Y. Zhao, L. Qu, ACS Nano 11 (2017) 5087–5093.
[64] S. Gruener, T. Hofmann, D. Wallacher, A.V. Kityk, P. Huber, Phys. Rev. E Stat. Nonlinear Soft Matter Phys. 79 (2009) 067301.
[65] K. Fu, Y. Yao, J. Dai, L. Hu, Adv. Mater. 29 (2017) 1603486.
[66] H. Wang, L. Miao, S. Tanemura, Sol. RRL 1 (2017) 1600023.
[67] M.S. Zielinski, J.W. Choi, T. La Grange, M. Modestino, S.M. Hashemi, Y. Pu, S. Birkhold, J.A. Hubbell, D. Psaltis, Nano Lett. 16 (2016) 2159–2167.
[68] Z. Fang, Y.R. Zhen, O. Neumann, A. Polman, F.J. Garcia de Abajo, P. Nordlander, N.J. Halas, Nano Lett. 13 (2013) 1736–1742.
[69] G. Ni, N. Miljkovic, H. Ghasemi, X. Huang, S.V. Boriskina, C.-T. Lin, J. Wang, Y. Xu, M.M. Rahman, T. Zhang, G. Chen, Nano Energy 17 (2015) 290–301.
[70] H. Jin, G. Lin, L. Bai, A. Zeiny, D. Wen, Nano Energy 28 (2016) 397–406.
[71] Z. Wang, Y. Liu, P. Tao, Q. Shen, N. Yi, F. Zhang, Q. Liu, C. Song, D. Zhang, W. Shang, T. Deng, Small 10 (2014) 3234–3239.
[72] X. Wang, Y. He, X. Liu, G. Cheng, J. Zhu, Appl. Energy 195 (2017) 414–425.
[73] C. Chang, C. Yang, Y. Liu, P. Tao, C. Song, W. Shang, J. Wu, T. Deng, ACS Appl. Mater. Interfaces 8 (2016) 23412–23418.
[74] S. Yu, Y. Zhang, H. Duan, Y. Liu, X. Quan, P. Tao, W. Shang, J. Wu, C. Song, T. Deng, Sci. Rep. 5 (2015) 13600.
[75] C. Liu, J. Huang, C.-E. Hsiung, Y. Tian, J. Wang, Y. Han, A. Fratalocchi, Adv. Sustain. Syst. 1 (2017) 1600013.
[76] L. Zhou, S. Zhuang, C. He, Y. Tan, Z. Wang, J. Zhu, Nano Energy 32 (2017) 195–200.
[77] L. Zhou, Y. Tan, D. Ji, B. Zhu, P. Zhang, J. Xu, Q. Gan, Z. Yu, J. Zhu, Sci. Adv. 2 (2016) e1501227.
[78] Y. Liu, J. Lou, M. Ni, C. Song, J. Wu, N.P. Dasgupta, P. Tao, W. Shang, T. Deng, ACS Appl. Mater. Interfaces 8 (2016) 772–779.
[79] A. Politano, P. Argurio, G. Di Profio, V. Sanna, A. Cupolillo, S. Chakraborty, H.A. Arafat, E. Curcio, Adv. Mater. 29 (2017), http://dx.doi.org/10.1002/adma.201603504.
[80] L. Tian, J. Luan, K.K. Liu, Q. Jiang, S. Tadepalli, M.K. Gupta, R.R. Naik, S. Singamaneni, Nano Lett. 16 (2016) 609–616.
[81] C. Boo, M. Elimelech, Nat. Nanotechnol. 12 (2017) 501–503.
[82] G. Liu, K. Wang, N. Hoivik, H. Jakobsen, Sol. Energy Mater. Sol. Cells 98 (2012) 24–38.
[83] X. Chen, L. Liu, P.Y. Yu, S.S. Mao, Science 331 (2011) 746–750.
[84] X. Chen, L. Liu, F. Huang, Chem. Soc. Rev. 44 (2015) 1861–1885.
[85] R. Li, L. Zhang, L. Shi, P. Wang, ACS Nano 11 (2017) 3752–3759.
[86] X. Liu, G. Zhu, X. Wang, X. Yuan, T. Lin, F. Huang, Adv. Energy Mater. 6 (2016) 1600452.
[87] Z. Wang, C. Yang, T. Lin, H. Yin, P. Chen, D. Wan, F. Xu, F. Huang, J. Lin, X. Xie, M. Jiang, Energy Environ. Sci. 6 (2013) 3007.
[88] G. Zhu, J. Xu, W. Zhao, F. Huang, ACS Appl. Mater. Interfaces 8 (2016) 31716–31721.
[89] X. Huang, I.H. El-Sayed, W. Qian, M.A. El-Sayed, J. Am. Chem. Soc. 128 (2006) 2115–2120.
[90] M.S. Yavuz, Y. Cheng, J. Chen, C.M. Cobley, Q. Zhang, M. Rycenga, J. Xie, C. Kim, K.H. Song, A.G. Schwartz, L.V. Wang, Y. Xia, Nat. Mater. 8 (2009) 935–939.
[91] Z. Hua, B. Li, L. Li, X. Yin, K. Chen, W. Wang, J. Phys. Chem. C 121 (2017) 60–69.
[92] G. Ni, G. Li, Svetlana V. Boriskina, H. Li, W. Yang, T. Zhang, G. Chen, Nat. Energy 1 (2016) 16126.
[93] B. Li, Q. Wang, R. Zou, X. Liu, K. Xu, W. Li, J. Hu, Nanoscale 6 (2014) 3274–3282.
[94] Y. Jiao, K. Liu, G. Wang, Y. Wang, X. Zhang, Chem. Sci. 6 (2015) 3975–3980.
[95] Z. Zha, X. Yue, Q. Ren, Z. Dai, Adv. Mater. 25 (2013) 777–782.
[96] M. Gryta, J. Membr. Sci. 287 (2007) 67–78.
[97] X. Huang, Y.H. Yu, Oscar L. de Llergo, S.M. Marquez, Z. Cheng, RSC Adv. 7 (2017) 9495–9499.
[98] H.G. Bahraseman, E.M. Languri, ASME-Power 2016 (2016) 59259.
[99] C. Silva, D. González, F. Suárez, Sol. Energy 142 (2017) 204–214.
[100] E. Shahraeeni, DISS. ETH No. 19404, 2010.

Guohua Liu received Ph.D. in Engineering of Thermophysics from Chinese Academy of Sciences in 2010. He obtained his 2nd Ph.D. in Micro and Nano Systems Technology at University College of Southeast Norway (HSN), 2013. Currently, he is a full professor at Nanjing University of Science and Technology. His research interests center on development and assembly of nanostructured materials for energy applications.

Jinliang Xu is the Dean of School of Mechanical and Power Engineering, North China Electric Power University, China. His research interest focuses on micro/nano heat transfer, micro energy system, and multiphase flow and heat transfer. He published more than 100 papers in recognized academic journals. He served as International conference chair or co-chair for several times in related area.

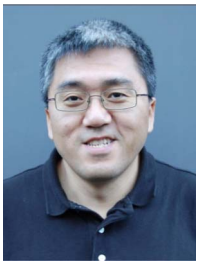

Kaiying Wang received Ph.D. in condensed matter physics from the Institute of Physics, Chinese Academy of Sciences in 1995. He had been a postdoc at University of New Orleans, USA. He joined University College of Southeast Norway in 2007 as an associate professor and then promoted as professor in 2010. His research interests focus on micro-fabrication and nanotechnology, functional thin films, magnetic and superconductive materials, nanostructure characterization and nanodevices for environment and energy applications.